

IMPROVING ACCURACY OF THE FIFTH-ORDER WENO SCHEME BY USING THE EXPONENTIAL APPROXIMATION SPACE

YOUNGSOO HA [§], CHANG HO KIM[‡], HYOSEON YANG [†], AND JUNGHO YOON [‡]

ABSTRACT. The aim of this study is to develop a novel WENO scheme that improves the performance of the well-known fifth-order WENO methods. The approximation space consists of exponential polynomials with a tension parameter that may be optimized to fit the the specific feature of the data, yielding better results compared to the polynomial approximation space. However, finding an optimal tension parameter is a very important and difficult problem, indeed a topic of active research. In this regard, this study introduces a practical approach to determine an optimal tension parameter by taking into account the relationship between the tension parameter and the accuracy of the exponential polynomial interpolation under the setting of the fifth-order WENO scheme. As a result, the proposed WENO scheme attains an improved order of accuracy (that is, sixth-order) better than other fifth-order WENO methods without loss of accuracy at critical points. A detailed analysis is provided to verify the improved convergence rate. Further, we present modified nonlinear weights based on L^1 -norm approach along with a new global smoothness indicator. The proposed nonlinear weights reduce numerical dissipation significantly, while attaining better resolution in smooth regions. Some experimental results for various benchmark test problems are presented to demonstrate the ability of the new scheme.

2000 AMS(MOS) Classification: 41A05, 41A10, 42A10, 65M06, 65M15

Keywords: Hyperbolic conservation laws, WENO scheme, exponential polynomial interpolation, tension parameter, order of accuracy, smoothness indicator.

1. INTRODUCTION

Hyperbolic systems are used for a wide range of scientific and engineering applications such as meteorology, gas dynamics, shallow water modeling, astrophysics models, and multiphase flow problems. It is well-known that the hyperbolic conservation laws may generate discontinuities in its solution even though the initial condition is smooth. Such discontinuities introduce undesirable artifacts like spurious oscillations in the numerical solutions. To avoid such phenomena, Total-Variation Diminishing (TVD) techniques have been developed [14, 15], but these schemes were revealed to have at most first-order accuracy. To overcome of this limitation, a series of essentially non-oscillatory (ENO) schemes have been developed. The ENO schemes [16, 17, 18, 36, 37] are designed to utilize several candidate stencils to avoid cross-shock interpolation such that they reduce spurious oscillations near discontinuities while achieving high order accuracy on smooth areas. The main idea of the weighted ENO (WENO) technique is to use a convex combination of all the candidate stencils of ENO in a nonlinear fashion and assigns a weight to each local solution based on its smoothness.

In [30], Liu et al. developed a weighted ENO scheme of a finite volume version which had the $(r + 1)$ -th order accuracy from the r th order ENO scheme on smooth regions using interpolating functions obtained from all candidate stencils in the ENO method. Later, Jiang and Shu [22] (called classical WENO or WENO-JS) introduced new smoothness indicators that measure the regularities of local solutions with

Date: February 17, 2020.

[§] Dept. of Math. Sciences, Seoul National University, Seoul, S. Korea (youngamath@snu.ac.kr), [‡] Dept. of Software Technology, Glocal Campus, Konkuk University, Chungju, S. Korea (kimchang@kku.ac.kr), [†] Dept. of Computational Mathematics, Science and Engineering, Michigan State University, East Lansing, MI, USA (hyoseon@msu.edu), [‡] Dept. of Math., Ewha Womans University, Seoul, S. Korea (yoon@ewha.ac.kr).

L^2 -norm to obtain the fifth-order accuracy on smooth regions. Although the WENO-JS possesses the fifth-order convergence rate in smooth regions, Henrick et al. noticed [19] that it suffers loss of accuracy near the critical points where the first and third derivatives do not vanish simultaneously. To correct this deficiency, the mapped WENO (hereafter, called WENO-M) scheme was devised in the form of a mapping function on the WENO-JS weights, leading to the maximal rate of convergence while achieving improved results near discontinuities [19]. Subsequently, Borges et al. [4] proposed another version of WENO schemes (called WENO-Z) by adding a new high order reference smoothness indicator consisting of a linear combination of the original smoothness indicator of WENO-JS. The WENO-M and WENO-Z schemes possess good shock capturing abilities, but both schemes fail to retain maximal order of accuracy near the high-order critical points [4]. Acker et al. [1] added a new term in the smoothness indicator to the fifth order WENO-Z weight to increase the relevance of less-smooth substencil such that it achieved better resolution in the smooth part of the solution while maintaining the same numerical stability as the original WENO-Z at shocks and discontinuities. Some other fifth-order WENO schemes were further proposed by modifying nonlinear weights [9, 12, 25, 49]. Sixth or higher order WENO techniques have been developed in the literature [3, 10, 13, 20, 21]. The central WENO [5, 24, 27], hybrid compact WENO schemes [32, 39], and other versions of the WENO methods [2, 6, 27, 28, 31, 46, 50] have been constructed to improve the performance of the WENO techniques.

The space of algebraic polynomials is the most well-established tool to reconstruct numerical flux. However, the interpolation method cannot be regulated according to the trait of the given data such that it causes excessive numerical dissipation when approximating rapidly varying data (e.g., sharp gradients or high oscillations). To circumvent this limitation, this study exploits the interpolation method based on the space of exponential polynomials of the form

$$\phi(x) = x^k e^{\lambda x}, \quad k \in \mathbb{Z}_+, \lambda \in \mathbb{R} \cup i\mathbb{R},$$

that allows an environment to fit the approximation to the characteristic of the given problem. For a given exponential polynomial space, the choice of the tension (or shape) parameter λ has a significant impact on the accuracy of interpolation. A well-selected parameter can yield better results compared to the polynomial-based method for various types of PDEs [11, 13, 45, 47, 48]. However, selecting an optimal parameter is an important and difficult problem, indeed a topic of active research. Most studies end up finding the tension parameter by using trial and error or minimization problem. In this regards, the goal of this study is first to present a specific type of exponential approximation space for the construction of numerical fluxes under the setting of the fifth-order WENO scheme. We then introduce a practical approach to determine an optimal parameter by taking into account the relation between the value of the tension parameter and the accuracy of the exponential polynomial interpolation. As a result, the proposed WENO scheme (termed as WENO-H) provides an improved order of accuracy better than the other fifth-order WENO methods. In fact, we will observe that the sixth-order accuracy can be achieved by the WENO-H technique, without loss of accuracy at critical points. A rigorous analysis is provided to prove the improved convergence rate. Further, a modified smoothness indicator based on L^1 -norm approach is presented along with a new global smoothness indicator. Accordingly, the proposed WENO scheme reduces numerical dissipation significantly, while attaining better resolution in smooth regions. Some experimental results for various benchmark test problems are given to illustrate the performance of the WENO-H scheme. The results are compared with those of some other methods to confirm the reliability of the proposed method.

The organization of the paper is as follows. Section 2 gives a brief review of the fifth-order WENO schemes for one-dimensional scalar conservation laws. In section 3, we propose a specific type of exponential approximation space and a practical approach to determine the parameter under the setting of the fifth-order WENO scheme. We also give a detailed analysis for the improved order of accuracy under a suitable condition of the tension parameter. In section 4, we introduce new modified smoothness indicators along with the associated WENO scheme. Finally, section 5 presents some experimental results to demonstrate the performance of the WENO-H. A conclusion is given in section 6.

2. WENO schemes

In this section we describe a general formulation of finite difference WENO schemes for solving hyperbolic conservation laws. Without loss of generality, we shall focus on the one-dimensional hyperbolic conservation laws which is given in the form

$$(1) \quad \begin{aligned} q_t + f(q)_x &= 0, \quad t \geq 0, \quad x \in \mathbb{R}, \\ q(x, 0) &= q_0(x), \end{aligned}$$

with suitable boundary conditions. Here, $q = (q_1, \dots, q_m)$ is a vector of conserved quantities, $f(q)$ is a vector-valued function with m components, and x and t indicate space and time variables respectively.

For simplicity of our presentation, we introduce some notation. The computational domain is assumed to be uniformly distributed with the cells $I_j = [x_{j-1/2}, x_{j+1/2}]$ and their centers x_j . The points $\{x_{j+1/2}\}$ are called the cell boundaries and the cell size is denoted by $\Delta x = x_{j+1/2} - x_{j-1/2}$. In particular, we use the notation f_j for the function value at the node x_j , i.e., $f_j := f(x_j)$. The set of nonnegative integers is denoted by \mathbb{Z}_+ , i.e., $\mathbb{Z}_+ = \{0\} \cup \mathbb{N}$.

2.1. Formulation of WENO scheme. At each node x_j , the semi-discretized form of the equation in (1) generates a system of ODE (ordinary differential equation) by the method of lines:

$$(2) \quad \frac{dq_j}{dt} = - \left. \frac{\partial f}{\partial x} \right|_{x=x_j}$$

with $q_j(t)$ an approximate value to the value $q(x_j, t)$ in a grid. Defining the flux function h implicitly by

$$(3) \quad f(q(x)) = \frac{1}{\Delta x} \int_{x-\Delta x/2}^{x+\Delta x/2} h(s) ds,$$

a conservative finite difference formulation constructs a numerical flux \hat{f} which approximates the function h at the cell boundaries with a high order of accuracy. Therefore, the spatial derivative $\left. \frac{\partial f}{\partial x} \right|_{x=x_j}$ in (2) can be represented as a discrete difference of the function h at the cell boundary $x_{j+1/2}$, which also can be exactly approximated by the following conservative scheme

$$(4) \quad \left. \frac{\partial f}{\partial x} \right|_{x=x_j} = \frac{h_{j+1/2} - h_{j-1/2}}{\Delta x}.$$

The interface numerical flux \hat{f} can be computed by

$$(5) \quad \hat{f}_{j+1/2} = Q(f_{j+1/2}^+, f_{j+1/2}^-)$$

where Q indicates a flux method. In practice, in order to ensure the numerical stability and avoid entropy violating solutions, the flux f is split into two components f^+ and f^- as $f(q) = f^+(q) + f^-(q)$. The interface limits f^- and f^+ are obtained by negative and positive parts of the flux $f(q)$, respectively. This study employs the Lax-Friedrichs splitting defined by

$$(6) \quad f^\pm(q) = \frac{1}{2}(f(q) \pm \alpha q),$$

where f^+ and f^- indicate the approximations to f from right and left respectively and $\alpha = \max_q |f'(q)|$ on the pertinent range of q .

2.2. Fifth-order WENO schemes. In the fifth-order WENO finite difference scheme, the numerical flux \hat{f} at the cell boundary $x_{j+1/2}$ in (5) is constructed on a 5-point stencil

$$\mathcal{S}_5 := \mathcal{S}(j) := \{x_{j-2}, x_{j-1}, x_j, x_{j+1}, x_{j+2}\}$$

which is subdivided into three candidate substencils $\mathcal{S}_k := \{x_{j+k-2}, \dots, x_{j+k}\}$, $k = 0, 1, 2$. Letting $\hat{f}_{j+1/2}^k$ be the local solution constructed on each substencil \mathcal{S}_k , the final WENO approximation is defined by a convex combination of these functions with weights ω_k :

$$\hat{f}_{j+1/2} = \sum_{k=0}^2 \omega_k \hat{f}_{j+1/2}^k.$$

To construct the weights ω_k , we first find the constants d_k which are called optimal (or ideal) weights such that its linear combination of $\hat{f}_{j+1/2}^k$ results in the central upwind fifth-order scheme to $h_{j+1/2}$. The specific values of d_k are known as $d_0 = 0.1$, $d_1 = 0.6$ and $d_2 = 0.3$ [35]. Then the nonlinear weights ω_k are defined by using these numbers d_k as follows:

$$\omega_k = \frac{\alpha_k}{\sum_{\ell=0}^2 \alpha_\ell}, \quad \alpha_k = \frac{d_k}{(\varepsilon + \beta_k)^2},$$

where a small positive value $\varepsilon > 0$ is employed to prevent the division by zero and $\omega_0 + \omega_1 + \omega_2 = 1$. The local smoothness indicator β_k estimates the regularity of the numerical flux \hat{f}^k which indeed determines to what extent the solution \hat{f}^k contributes to the final WENO reconstruction. The smoothness indicators introduced by Jiang and Shu [22] are given by

$$(7) \quad \beta_k = \sum_{\ell=1}^2 \int_{x_{j-1/2}}^{x_{j+1/2}} \Delta x^{2\ell-1} \left(\frac{d^\ell}{dx^\ell} \hat{f}^k \right)^2 dx.$$

The scheme is called WENO-JS. It was noted that the WENO-JS achieves only the third order accuracy at critical points. To correct this drawback, two different WENO techniques have been developed. Henrick et al. [19] suggested a modified fifth-order WENO method (WENO-M) by using a mapping procedure to the smoothness indicators to recover the maximal convergence rate (7). Later, Borges et al. [4] introduced another approach for the WENO scheme (referred to as WENO-Z) by using a global high order smoothness indicator which makes the nonlinear weights converge to the optimal weights faster than the classical WENO scheme.

3. Interpolation based on exponential polynomial basis functions

3.1. Exponential Function Space. Although the space of polynomials is most commonly used to implement numerical fluxes, the interpolation method causes excessive numerical dissipation when approximating rapidly varying data. In order to make up for this weakness, we employ a method based on exponential polynomials of the form

$$(8) \quad \phi(x) = x^k e^{\lambda x}, \quad k \in \mathbb{Z}_+, \quad \lambda \in \mathbb{R} \cup i\mathbb{R}.$$

If $k = 0$ and λ is pure imaginary, the function ϕ becomes a trigonometric polynomial. The motivation of using this type of functions is to exploit λ as a tension parameter so that it allows one to choose an optimized parameter to fit the specific features of the solution.

Let $\mathbb{B}_m := \{\phi_1, \dots, \phi_m\}$ with $m \in \mathbb{N}$ be a set of exponential polynomials. When the set \mathbb{B}_m constitutes an *extended Tchebysheff system* on \mathbb{R} , the non-singularity of the interpolation matrix is guaranteed [23]. Practically, for a given cell boundary $x_{j+1/2}$, we look for the approximate solution from the shifted function space

$$(9) \quad \Gamma_m := \text{span}\{\phi_n(\cdot - x_{j+1/2}) : \phi_n \in \mathbb{B}_m\}$$

to avoid using large numbers in the interpolation matrix. The construction of the numerical flux \hat{f} based on \mathbb{B}_5 complies with the methodology of the central-upwind schemes. We use an m -point stencil to construct

\hat{f} approximating the flux h with the m th convergence order at the cell interface. That is, from a given set of cell-average values on the stencil, the function \hat{f} is defined as follows

$$(10) \quad h \approx \hat{f} = \sum_{n=1}^m a_n \phi_n(\cdot - x_{j+1/2}) \in \Gamma_m$$

with the coefficients a_k obtained by evaluating the integral at the stencil nodes [13, 19]. Equivalently, a convenient way to construct the numerical flux \hat{f} is via Lagrange's interpolation formula to the primitive function H of h on the cell-boundaries (say $\mathcal{S}_m^b := \{x_{j-r-1/2}, \dots, x_{j-r+m-1/2}\}$ for some $r \in \mathbb{Z}_+$), that is,

$$\hat{f}_{j+1/2} := \sum_{n=0}^m L'_n(x_{j+1/2}) H(x_{j-r+n-1/2}).$$

In actual computation, the function H need not to be computed explicitly. The values of H at the cell boundaries can be computed directly by using the given cell-average values. Letting $\mathbb{B}_m^b = \{\varphi_0, \dots, \varphi_m\}$ be a set of exponential polynomials such that $\Gamma_m = \text{span}\{\varphi'_k(\cdot - x_{j+1/2}) : \varphi_k \in \mathbb{B}_m^b\}$, the Lagrange functions L_n are in fact determined by solving the linear system

$$(11) \quad \sum_{n=0}^m L_n(x) \varphi_\ell(x_{j-r+\ell-1/2} - x_{j+1/2}) = \varphi_\ell(x), \quad \forall \varphi_\ell \in \mathbb{B}_m^b,$$

which means the exponential polynomial reproducing property of $\{L_n\}$. It is obvious that each L'_n belongs to the space Γ_m for $n = 0, \dots, m$.

Remark 3.1. When $\varphi_n(x) = x^n$ for $n = 0, \dots, m$, the solution of the linear system in (11) is uniquely determined by the set of the Lagrange polynomials (denoted by $\{u_n : n = 0, \dots, m\}$) of degree m on S_m^b which fulfills the polynomial reproducing property

$$(12) \quad \sum_{n=0}^m u_n^{(\alpha)}(x) p(x_{j-r+n-1/2}) = p^{(\alpha)}(x), \quad \forall p \in \Pi_m.$$

For later use, we introduce the dilation of u_n that is, $\bar{u}_n := u_n(\Delta x \cdot)$, which are the Lagrange polynomials on the stencil $\{-r - \frac{1}{2}, \dots, -r + m - \frac{1}{2}\}$. It is necessary to remark that the Lagrange polynomials are shift-invariant so that $\bar{u}_n(1/2) = u_n(x_{j+1/2})$.

The relation between L_n and u_n is treated in the following Lemma 3.2, which is useful for our further analysis. In fact, the specific proof can be obtained similarly as in the proof of [11, Theorem 3]. But, in order to make this paper self-contained, the proof is sketched briefly here.

Lemma 3.2. *Let $\mathbf{L}(x) = (L_n(x) : n = 0, \dots, m)$ and $\mathbf{U}(x) = (u_n(x) : n = 0, \dots, m)$ be the vectors of Lagrange functions in (11) and (12) respectively. Then, for any $\alpha = 0, \dots, m-1$, we have*

$$\|\mathbf{L}^{(\alpha)}(x_{j+1/2}) - \mathbf{U}^{(\alpha)}(x_{j+1/2})\|_\infty = \mathcal{O}(\Delta x).$$

Proof. For notational simplicity, put $\bar{x} = x_{j+1/2}$. Let T_{φ_k} be the Taylor polynomial of $\varphi_k(\cdot - \bar{x})$ up to degree m around \bar{x} , i.e.,

$$T_{\varphi_k} = \sum_{\ell=0}^m (\cdot - \bar{x})^\ell \phi_k^{(\ell)}(0) / \ell!,$$

and let \mathbf{T} be the matrix with components $\mathbf{T}(k, n) = T_{\varphi_k}(x_{j-r+n-1/2})$ for $k, n = 0, \dots, m$. Further, letting \mathbf{D} be the diagonal matrix with the entries $\mathbf{D} = \text{diag}(\Delta x^k : k = 0, \dots, m)$, the matrix \mathbf{T} can be written as

$$\mathbf{T} = \mathbf{W} \cdot \mathbf{D} \cdot \mathbf{V}$$

with

$$\mathbf{W} = (\varphi_k^{(\ell)}(0) : k, \ell = 0, \dots, m), \quad \mathbf{V} = ((-r + n - 1)^\ell / \ell! : \ell, n = 0, \dots, m).$$

Here \mathbf{V} is a Vandermonde matrix and \mathbf{W} is the Wronskian matrix of \mathbb{B}_5 so that their non-singularities are clear. Using this expression, the linear system in (11) which in fact uniquely determines the solution $\mathbf{L}(\bar{x})$ can be decomposed into the form

$$(\mathbf{V} + \Delta x \mathbf{R}) \mathbf{L}^{(\alpha)}(\bar{x}) = \mathbf{p}^{(\alpha)}(\bar{x}) + \Delta x \mathbf{r}^{(\alpha)}(\bar{x})$$

with $\mathbf{p}^{(\alpha)}(\bar{x}) = (\delta_{\alpha,n} : n = 0, \dots, m)^T$ for some matrices \mathbf{R} and $\mathbf{r}(x)$ with $\|\mathbf{R}\|_\infty, \|\mathbf{r}\|_\infty \leq c_1 < \infty$. It is well-known (e.g., see [8]) that a $\mathcal{O}(\Delta x)$ perturbation of a non-singular matrix results in also the $\mathcal{O}(\Delta x)$ perturbation of its inverse matrix. Thus, it follows that

$$\begin{aligned} \mathbf{L}^{(\alpha)}(\bar{x}) &= (\mathbf{V} + \Delta x \mathbf{R})^{-1} (\mathbf{p}^{(\alpha)}(\bar{x}) + \Delta x \mathbf{r}^{(\alpha)}(\bar{x})) \\ &= (\mathbf{V}^{-1} + \Delta x \tilde{\mathbf{R}}) (\mathbf{p}^{(\alpha)}(\bar{x}) + \Delta x \mathbf{r}^{(\alpha)}(\bar{x})) \\ &= \mathbf{V}^{-1} \mathbf{p}^{(\alpha)}(\bar{x}) + \mathcal{O}(\Delta x). \end{aligned}$$

In view of (12), $\mathbf{V}^{-1} \mathbf{p}^{(\alpha)}(\bar{x}) = \mathbf{U}^{(\alpha)}(\bar{x})$. It leads to $\|\mathbf{L}^{(\alpha)}(\bar{x}) - \mathbf{U}^{(\alpha)}(\bar{x})\|_\infty = \mathcal{O}(\Delta x)$, which completes the proof. \square

3.2. Optimal tension parameter. The goal of this section is two folds. We first propose a specific type of exponential approximation space for the construction of numerical fluxes under the setting of the fifth-order WENO scheme. This study is particularly interested in the following set of functions

$$(13) \quad \mathbb{B}_5 := \{1, x, x^2, \phi_3(x), \phi_4(x)\},$$

where ϕ_3 and ϕ_4 are exponential polynomials. In this study, we will mainly concentrate on the case

$$\phi_3(x) = \sinh \lambda x, \quad \phi_4(x) = \cosh \lambda x.$$

As discussed before, for a given cell-boundary $x_{j+1/2}$, the approximate solution on \mathcal{S}_5 is obtained from the space

$$I_5 = \text{span}\{\phi_i(\cdot - x_{j+1/2}) : \phi_i \in \mathbb{B}_5\}$$

to avoid using large numbers in interpolation process. Then our next goal is to present a practical approach to find the parameter λ without any trial and error or minimization process. For this purpose, we take into account the relation between the parameter λ and the convergence behavior of the approximation to the spartial derivative $\partial f / \partial x$ at $x = x_j$ in (4), i.e.,

$$(14) \quad \mathcal{E}_j := \frac{\partial f}{\partial x} \Big|_{x=x_j} - \frac{\hat{f}_{j+1/2} - \hat{f}_{j-1/2}}{\Delta x}.$$

Our specific selection of ϕ_n ($n = 3, 4$) and the associated tension parameter is presented below in terms of the primitive function H of the flux h . In actual computation, the values of H at the cell boundaries can be computed directly by using the given cell-average values:

$$(15) \quad H(x_{n+1/2}) = \Delta x \sum_{\ell=j-2}^n \bar{h}_\ell.$$

We then verify that for a suitably chosen parameter, the corresponding interpolation method can improve the rate of accuracy of the classical polynomial interpolation method.

Remark 3.3. Prior to further study, it is worthwhile to point out that if $|H^{(6)}(x)| = 0$ (or practically, $|H^{(6)}(x)| \leq \bar{c} \Delta x^2$ for a fixed constant $c > 0$), the interpolation method provides an improved accuracy of \mathcal{E}_j for any suitable set \mathbb{B}_5 (including algebraic polynomials); see Proposition 3.11. In this case, one may use the classical interpolation method based on polynomials to construct $\hat{f}_{j+1/2}$. In this view point, in what follows, it is reasonable to consider the case $H^{(6)}(x) \neq 0$.

• **Central Condition A.** For a given cell boundary $x_{j+1/2}$, without great loss, we suppose that $H^{(n)}(x_{j+1/2})$ does not vanish simultaneously for both $n = 4, 5$. Then, exponential approximation space is chosen by considering the following two cases:

C1: If $H^{(4)}(x_{j+1/2})$ is non-zero, we set

$$\mathbb{B}_5 = \{1, x, x^2, \sinh \lambda x, \cosh \lambda x\}$$

with the tension parameter λ satisfying the condition

$$\lambda^2 = \left(\frac{H^{(6)}}{H^{(4)}} \right) (x_{j+1/2}) + O(\Delta x).$$

In practice, as long as the flux f is not constant or linear (more generally, polynomially changing) around $x_{j+1/2}$, $H^{(4)}$ is nonzero almost everywhere. Hence, in this study, we are mainly concentrating on the case C1. But, if this is not the case, it is treated by the case C2.

C2: If $H^{(4)}(x_{j+1/2}) = 0$ and $H^{(5)}(x_{j+1/2})$ is nonzero, we set

$$\mathbb{B}_5 = \left\{ 1, x, x^2, \sinh \lambda x, \cosh \lambda x + \frac{\lambda^6 x^5}{5!} \right\}$$

with the tension parameter λ satisfying the condition

$$\lambda^2 = \left(\frac{H^{(6)}}{H^{(5)}} \right) (x_{j+1/2}) + O(\Delta x).$$

Remark 3.4. For the construction of local numerical flux on each substencil \mathcal{S}_k for $k = 0, 1, 2$, we use the algebraic polynomials, i.e.,

$$\mathbb{B}_3 = \{1, x, x^2\}.$$

It means that the reconstruction of the local solution on each substencil \mathcal{S}_k is exactly the same as the case of the classical fifth-order WENO method.

3.3. Improved approximation order by exponential polynomials. We now prove that the proposed interpolation method based on the ‘Central Condition A’ provides an improved accuracy compared to other fifth-order WENO schemes. To do this, let $\mathbb{B}_5^b = \{\varphi_0, \dots, \varphi_5\}$ be a set of exponential polynomials such that $\Gamma_5 = \text{span}\{\varphi'_k(\cdot - x_{j+1/2}) : k = 0, \dots, 5\}$. Then the numerical flux \hat{f} is defined through the Lagrangian interpolation formula to the function H on the cell-boundaries $\mathcal{S}_5^b := \{x_{j-5/2}, \dots, x_{j+5/2}\}$, that is,

$$(16) \quad \hat{f}_{j+1/2} := \sum_{n=0}^5 L'_n(x_{j+1/2}) H(x_{n+j-5/2}).$$

First consider the case ‘C1’. The case ‘C2’ follows later.

• **Case I:** $H^{(4)}(x_{j+1/2})$ is non-zero.

Recalling that $\mathbb{B}_5 = \{1, x, x^2, \sinh \lambda x, \cosh \lambda x\}$, let $\mathbb{B}_5^b = \{\varphi_0, \dots, \varphi_5\}$ be a set of exponential polynomials such that $\Gamma_5 = \text{span}\{\varphi'_n(\cdot - x_{j+1/2}) : \varphi_n \in \mathbb{B}_5^b\}$. To facilitate our further analysis for the convergence order of the proposed method, we reorganize the elements in \mathbb{B}_5^b as follows:

$$\begin{aligned} \varphi_n(x) &= x^n/n! \quad (n = 0, \dots, 3), \\ \varphi_4(x) &= \frac{1}{\lambda^4} \left(\cosh(\lambda x) - 1 - \frac{(\lambda x)^2}{2} \right), \quad \varphi_5(x) = \frac{1}{\lambda^5} \left(\sinh(\lambda x) - \lambda x - \frac{(\lambda x)^3}{3!} \right). \end{aligned}$$

It is obvious that each function $\varphi'_n(\cdot - x_{j+1/2})$ belongs to the space Γ_5 . Then, by a linear combination of these functions, we define an auxiliary function ψ as follows:

$$(17) \quad \psi := \psi_j := \sum_{n=0}^5 \mu_{j,n} \varphi_n(\cdot - x_{j+1/2})$$

with the coefficient vector $\boldsymbol{\mu} = (\mu_{j,n} : n = 0, \dots, 5)^T$ obtained by solving the linear system

$$(18) \quad \psi^{(n)}(x_{j+1/2}) = H^{(n)}(x_{j+1/2}), \quad n = 0, \dots, 5.$$

The following lemma treats the uniqueness of the solution $\boldsymbol{\mu}$ and also finds its explicit form.

Lemma 3.5. *Let ψ be defined as in (17) with the coefficient vector $\boldsymbol{\mu} = (\mu_{j,n} : n = 0, \dots, 5)^T$. Then, there exists a unique solution $\boldsymbol{\mu}$ with the form $\mu_{j,n} = H^{(n)}(x_{j+1/2})$ for $n = 0, \dots, 5$.*

Proof. Let $\mathbf{W}_0 := (\varphi_n^{(\ell)}(0) : \ell, n = 0, \dots, 5)$ be the Wronskian matrix of $\{\varphi_0, \dots, \varphi_5\}$ at 0 and let $\mathbf{H}_j := (H^{(\ell)}(x_{j+1/2}) : \ell = 0, \dots, 5)$. Note that the vector $\boldsymbol{\mu}$ can be rewritten in the following matrix form

$$\mathbf{W}_0 \cdot \boldsymbol{\mu} = \mathbf{H}_j.$$

Since \mathbf{W}_0 is non-singular, the uniqueness of the solution $\boldsymbol{\mu}$ is obvious. In fact, an elementary calculation reveals that $\varphi_n^{(\ell)} = \delta_{\ell,n}$ with $\delta_{\ell,n}$ the Kronecker delta, which means that \mathbf{W}_0 the identity matrix. Thus, the lemma is proved immediately. \square

We now prove the convergence order of the approximation to the spatial derivative $\partial f / \partial x$ in (14). This study is especially interested in approximating functions g in the Sobolev space

$$W_\infty^k(\Omega) := \{g \in C^{(k)}(\Omega) : \|g^{(k)}\|_{L^\infty(\Omega)} < \infty\}$$

where Ω is an open set in \mathbb{R} . For this proof, we recall that g_j indicates the value $g(x_j)$ at the node x_j . Also, denote by T_g the Taylor polynomial of degree 5 around $x_{j+1/2}$ of the function g , i.e.,

$$(19) \quad T_g := T_{g, x_{j+1/2}} := \sum_{n=0}^5 (\cdot - x_{j+1/2})^n g^{(n)}(x_{j+1/2}).$$

Theorem 3.6. *Assume that $H \in W_\infty^7(\Omega)$ with Ω an open neighborhood of $x_{j+1/2}$. Let \hat{f} be the numerical flux defined as in (16). Then, under the ‘Central Condition A-C1’, we have*

$$(20) \quad h(x_{j\pm 1/2}) - \hat{f}(x_{j\pm 1/2}) = C_j \Delta x^6 + \mathcal{O}(\Delta x^7)$$

with

$$(21) \quad C_j = \left(\frac{H^{(5)} H^{(6)}}{H^{(4)}} - H^{(7)} \right) (x_j) \sum_{n=0}^5 \bar{u}'_n(1/2) (n-3)^7 / 7!.$$

where \bar{u}_n are the Lagrange polynomials of degree 5 on the stencil $\{-5/2, \dots, 5/2\}$.

Proof. In this proof, we first analyze the accuracy of \hat{f} to the function h at $x_{j+1/2}$. To do this, we employ the auxiliary function ψ defined in (17). Due to the condition in (18), $\psi'(x_{j+1/2}) = H'(x_{j+1/2})$. Also, since H is the primitive function of h , $H'(x_{j+1/2}) = h_{j+1/2}$. It implies that $h_{j+1/2} = \psi'(x_{j+1/2})$. Then using the formula of the numerical flux $\hat{f}_{j+1/2}$ in (16), we can write

$$(22) \quad h_{j+1/2} - \hat{f}_{j+1/2} = \psi'(x_{j+1/2}) - \sum_{n=0}^5 L'_n(x_{j+1/2}) H(x_{n+j-5/2}).$$

Further, since the derivative ψ' belongs to the space Γ_5 , in view of the exponential polynomial reproducing property in (11), we can express

$$\psi'(x_{j+1/2}) = \sum_{n=0}^5 L'_n(x_{j+1/2}) \psi(x_{n+j-5/2}).$$

Combining this with (22) derives the equation

$$(23) \quad h_{j+1/2} - \hat{f}_{j+1/2} = \sum_{n=0}^5 L'_n(x_{j+1/2}) (\psi(x_{n+j-5/2}) - H(x_{n+j-5/2})).$$

Next, to estimate the difference $\psi(x_{n+j-5/2}) - H(x_{n+j-5/2})$ in the above equation, we use the Taylor expansion argument. In fact, since $\psi^{(\ell)}(x_{j+1/2}) = H^{(\ell)}(x_{j+1/2})$ for $\ell = 0, \dots, 5$, it is apparent that

$$T_\psi = T_H$$

with T_g the Taylor polynomial of g in (19). Accordingly, it holds that

$$(24) \quad \psi(x_{n+j-5/2}) - H(x_{n+j-5/2}) = R_\psi(x_{n+j-5/2}) - R_H(x_{n+j-5/2})$$

where R_g is the remainder of the Taylor polynomial T_g . Then, in order to get an improved convergence rate of the difference $h_{j+1/2} - \hat{f}_{j+1/2}$, we would like to verify that

$$\psi_j^{(6)}(x_{j+1/2}) = H^{(6)}(x_{j+1/2})$$

under the ‘Central Condition A-C1’. Indeed, from the formula of ψ in (18) and Lemma 3.5, a direct calculation yields the identity $\psi_j^{(6)}(x_{j+1/2}) = \lambda^2 H^{(4)}(x_{j+1/2})$, where $H^{(4)}(x_{j+1/2})$ is non-zero by assumption. Thus, putting

$$(25) \quad \lambda^2 = H^{(6)}(x_{j+1/2})/H^{(4)}(x_{j+1/2}),$$

we prove that $\psi^{(6)}(x_{j+1/2}) = H^{(6)}(x_{j+1/2})$. Consequently, using the explicit formula of the remainder terms of ψ and H , it holds immediately from (24) that

$$(26) \quad \psi(x_{n+j-5/2}) - H(x_{n+j-5/2}) = \Delta x^7 \frac{(n-3)^7}{7!} (\psi^{(7)} - H^{(7)})(x_{j+1/2}) + O(\Delta x^8).$$

Moreover, from the definition of ψ , we calculate that $\psi^{(7)}(x_{j+1/2}) = \lambda^2 H^{(5)}(x_{j+1/2})$. Substituting the value λ in (25) into this equation results in the expression

$$\psi^{(7)}(x_{j+1/2}) = \frac{H^{(5)}H^{(6)}}{H^{(4)}}(x_{j+1/2}).$$

Applying the mean-value theorem, it follows that

$$(27) \quad (\psi^{(7)} - H^{(7)})(x_{j+1/2}) = \left(\frac{H^{(5)}H^{(6)}}{H^{(4)}} - H^{(7)} \right)(x_j) + O(\Delta x), \quad \text{as } \Delta x \rightarrow 0.$$

On the other hand, let us recall from Lemma 3.2 that $L'_n(x_{j+1/2}) = u'_n(x_{j+1/2}) + \mathcal{O}(\Delta x)$ with u_n the Lagrange polynomial of degree 5 on the stencil \mathcal{S}_5^b as in (12). Also, $\sum_{n=0}^5 |u'_n(x_{j+1/2})| \leq c\Delta x^{-1}$. Combining these arguments with (23), (26) and (27), we arrive at the expression

$$h_{j+1/2} - \hat{f}_{j+1/2} = \Delta x^7 \sum_{n=0}^5 u'_n(x_{j+1/2}) \frac{(n-3)^7}{7!} \left(\frac{H^{(5)}H^{(6)}}{H^{(4)}} - H^{(7)} \right)(x_j) + O(\Delta x^7).$$

Now, let $\bar{u}_n := u_n(\Delta x \cdot)$ be the dilation of u_n , that is, the Lagrange polynomials on the stencil $\{-\frac{5}{2}, \dots, \frac{5}{2}\}$ as discussed in Remark 3.1. Clearly, $\bar{u}'_n = \Delta x u'_n(\Delta x \cdot)$ such that $u'(x_{j+1/2}) = \Delta x^{-1} \bar{u}'_n(1/2)$. Therefore, we conclude that

$$(28) \quad h_{j+1/2} - \hat{f}_{j+1/2} = C_j \Delta x^6 + O(\Delta x^7)$$

with C_j defined in (21), which is the required result of this theorem. Moreover, to estimate $\hat{f}_{j-1/2}$, the stencil \mathcal{S}_5 used to compute $\hat{f}_{j+1/2}$ is moved by one-grid to the left. Since the Lagrange polynomials are shift-invariant, we can prove (20) by applying the same technique. The proof is completed. \square

Corollary 3.7. *Assume that $H \in W_\infty^7(\Omega)$ with Ω an open neighborhood of $x_{j+1/2}$. Let \hat{f} be the numerical flux defined as in (16). Then, under the Central Condition A-C1, we have*

$$\mathcal{E}_j(f) = \frac{h_{j+1/2} - h_{j-1/2}}{\Delta x} - \frac{\hat{f}_{j+1/2} - \hat{f}_{j-1/2}}{\Delta x} = O(\Delta x^6)$$

Proof. The term $C_j \Delta x^6$ in (20) is the same for both $h_{j+1/2} - \hat{f}_{j+1/2}$ and $h_{j-1/2} - \hat{f}_{j-1/2}$. Thus, putting the result of Lemma (3.6) at the finite difference formula $\mathcal{E}_j(f)$ in (3.6), we find that Δx^6 term remains after division by Δx . Thus, the theorem holds immediately. \square

• **Case II:** $H^{(4)}(x_{j+1/2}) = 0$ and $H^{(5)}(x_{j+1/2})$ is non-zero.

The general approach for this case is similar to the Case I, but we have to modify it to meet the condition $H^{(4)}(x_{j+1/2}) = 0$ and $H^{(5)}(x_{j+1/2}) \neq 0$. For this purpose, as before, we employ an auxiliary function ψ defined by a linear combination of the functions in \mathbb{B}_5^b . As in the case of C1, we reorganize the elements in \mathbb{B}_5^b as follows:

$$\begin{aligned} \varphi_n(x) &= x^n/n!, \quad (n = 0, \dots, 3), \\ \varphi_4(x) &= \frac{1}{\lambda^4} \left(\cosh(\lambda x) - 1 - \frac{(\lambda x)^2}{2} \right), \quad \varphi_5(x) = \frac{1}{\lambda^5} \left(\sinh(\lambda x) - \lambda x - \frac{(\lambda x)^3}{3!} \right) + \frac{\lambda^2 x^6}{6!}. \end{aligned}$$

It is not difficult to see that $\varphi'_n(\cdot - x_{j+1/2}) \in \Gamma_5$. Compared to the Case I, we note that only the function φ_5 is defined differently. We then introduce an auxiliary ψ by

$$(29) \quad \psi := \psi_j(x) := \sum_{n=0}^5 \mu_{j,n} \varphi_n(\cdot - x_{j+1/2})$$

with the coefficient vector $\boldsymbol{\mu}$ satisfying the linear system

$$(30) \quad \psi^{(\ell)}(x_{j+1/2}) = H^{(\ell)}(x_{j+1/2}), \quad \ell = 0, \dots, 5.$$

The uniqueness of the solution $\boldsymbol{\mu}$ and its explicit form are discussed below.

Lemma 3.8. *Let ψ be defined as in (29) with the coefficient vector $\boldsymbol{\mu} = (\mu_{j,n} : n = 0, \dots, 5)^T$. Then, there exists a unique solution $\boldsymbol{\mu}$ with the form $\mu_{j,n} = H^{(n)}(x_{j+1/2})$ for $n = 0, \dots, 5$.*

Proof. Let $\mathbf{W}_0 := (\varphi_n^{(\ell)}(0) : \ell, n = 0, \dots, 5)$ be the Wronskian matrix of $\{\varphi_0, \dots, \varphi_5\}$ at 0. It can be easily checked that \mathbf{W}_0 is the identity matrix. Thus, the same technique in Lemma 3.5 can be applied to prove $\boldsymbol{\mu} = \mathbf{H}_j$ with $\mathbf{H}_j := (H^{(\ell)}(x_{j+1/2}) : \ell = 0, \dots, 5)$. \square

Theorem 3.9. *Assume that $H \in W_\infty^7(\Omega)$ with Ω an open neighborhood of $x_{j+1/2}$. Let \hat{f} be the numerical flux defined as in (16). Then, under the Central Condition A-C2, we have*

$$(31) \quad h(x_{j\pm 1/2}) - \hat{f}(x_{j\pm 1/2}) = C_j \Delta x^6 + \mathcal{O}(\Delta x^7)$$

with

$$C_j = (H^{(6)} - H^{(7)})(x_j) \sum_{n=0}^5 \bar{u}'_n(1/2) (n-3)^7 / 7!,$$

where \bar{u}_n are the Lagrange polynomials on the stencil $\{-\frac{5}{2}, \dots, \frac{5}{2}\}$.

Proof. The general technique for this proof is similar to that for Theorem 3.6. Therefore, it is sketched here by pointing out the crucial different parts. First, since the function ψ' in (29) belongs to the space Γ_5 , as in the proof of Theorem 3.6, we can write

$$(32) \quad h(x_{j+1/2}) - \hat{f}(x_{j+1/2}) = \sum_{n=0}^5 L'_n(x_{j+1/2}) (\psi(x_{n+j-5/2}) - H(x_{n+j-5/2})).$$

Then, to estimate the term $\psi(x_{n+j-5/2}) - H(x_{n+j-5/2})$ of the above equation, we exploit the Taylor expansion argument and the condition $\psi^{(\ell)}(x_{j+1/2}) = H^{(\ell)}(x_{j+1/2})$ with $\ell = 0, \dots, 5$ such that it leads to the expression

$$(33) \quad \psi(x_{n+j-5/2}) - H(x_{n+j-5/2}) = R_\psi(x_{n+j-5/2}) - R_H(x_{n+j-5/2}).$$

Now, in order to obtain an improved convergence rate in (32), we discuss the condition of the parameter λ that makes $\psi^{(6)}(x_{j+1/2}) = H^{(6)}(x_{j+1/2})$. Indeed, due to Lemma 3.8 and the condition of ψ , a direct calculation yields the equation

$$\psi^{(6)}(x_{j+1/2}) = \lambda^2(H^{(4)} + H^{(5)})(x_{j+1/2}) = \lambda^2 H^{(5)}(x_{j+1/2})$$

because $H^{(4)}(x_{j+1/2}) = 0$. By assumption, $H^{(5)}(x_{j+1/2})$ is non-zero. Hence, putting

$$(34) \quad \lambda^2 = H^{(6)}(x_{j+1/2})/H^{(5)}(x_{j+1/2}),$$

induces the equation $\psi^{(6)}(x_{j+1/2}) = H^{(6)}(x_{j+1/2})$. Also, using (34) and by the definition of ψ , we obtain $\psi^{(7)}(x_{j+1/2}) = H^{(6)}(x_{j+1/2})$. Therefore, following the same techniques in the proof of Theorem 3.9, we can finish the proof. \square

As in Corollary 3.7, we get the following result.

Corollary 3.10. *Assume that $H \in W_\infty^7(\Omega)$ with Ω an open neighborhood of $x_{j+1/2}$. Let \hat{f} be the numerical flux defined as in (16). Then, under the Central Condition A-C2, we have*

$$\frac{\partial f}{\partial x} \Big|_{x=x_j} - \frac{\hat{f}_{j+1/2} - \hat{f}_{j-1/2}}{\Delta x} = O(\Delta x^6).$$

As mentioned in Remark 3.3, when $H^{(6)}(x_{j+1/2}) = 0$ or $|H^{(6)}(x_{j\pm 1/2})| \leq \bar{c}\Delta x^2$, the interpolation method provides an improved accuracy of \mathcal{E}_j for any choice of \mathbb{B}_5 (including algebraic polynomials). Next proposition treats this case.

Proposition 3.11. *Suppose that $|H^{(6)}(x_{j\pm 1/2})| \leq \bar{c}\Delta x^2$ for a fixed constant $\bar{c} > 0$. Then for any choice of the set \mathbb{B}_5 in the ‘Central Condition A’ or $\mathbb{B}_5 = \{1, \dots, x^4\}$, we have the estimate $|\mathcal{E}_j(f)| = \mathcal{O}(\Delta x^6)$ as $\Delta x \rightarrow 0$.*

Proof. We first consider the case that $\hat{f}_{j+1/2}$ is constructed by using the classical polynomial interpolation method. Let T_H be the Taylor polynomial of H around $x_{j+1/2}$ of degree 5 and write $H = T_H + R_H$ with R_H the remainder of the Taylor polynomial T_H . Then, due to the polynomial reproducing property of the Lagrange polynomials $\{u_n : n = 0, \dots, 5\}$ in (12), we have

$$(35) \quad \begin{aligned} \hat{f}_{j+1/2} &= \sum_{n=0}^5 u'_n(x_{j+1/2})(T_H + R_H)(x_{n+j-5/2}) \\ &= T'_H(x_{j+1/2}) + \sum_{n=0}^5 u'_n(x_{j+1/2})R_H(x_{n+j-5/2}). \end{aligned}$$

Obviously, $T'_H(x_{j+1/2}) = H'(x_{j+1/2})$ and $H'(x_{j+1/2}) = h(x_{j+1/2})$ because H is the primitive function of h . Also, by assumption, $|H^{(6)}(x_{j+1/2})| \leq \bar{c}\Delta x^2$ and $H^{(7)}(x_{j+1/2}) = |H^{(7)}(x_j)| + \mathcal{O}(\Delta x)$. It implies that the remainder R_H is the form

$$(36) \quad R_H = (\cdot - x_{j+1/2})^7 H^{(7)}(x_j)/7! + \mathcal{O}(\Delta x^8).$$

Since $u'_n(x_{j+1/2}) = \Delta x^{-1}\bar{u}'_n(1/2)$ with \bar{u}_n the Lagrange polynomials on the stencil $\{-\frac{5}{2}, \dots, \frac{5}{2}\}$, in view of these arguments with (35) and (36), it holds immediately that

$$(37) \quad h_{j+1/2} - \hat{f}_{j+1/2} = C_j \Delta x^6 + \mathcal{O}(\Delta x^7)$$

with the constant C_j defined by

$$(38) \quad C_j = - \sum_{n=0}^5 \bar{u}'_n(1/2) \frac{(n-3)^7}{7!} H^{(7)}(x_j).$$

Second, suppose that $\hat{f}_{j+1/2}$ is obtained from the space spanned by the set \mathbb{B}_5 either in the case ‘C1’ or ‘C2’. Since $|H^{(6)}(x_{j\pm 1/2})| \leq \bar{c}\Delta x^2$, a direct calculation from the definition of ψ and the value of λ in the ‘Central Condition A’ yields the bound $|\psi^{(7)}(x_{j+1/2})| \leq c|\lambda|^2 \leq c\Delta x$. It leads to the same estimate in (37). Therefore, following the same methodology in the proof of Corollary 3.7, we can get the required result $|\mathcal{E}_j(f)| = \mathcal{O}(\Delta x^6)$. The proof is completed. \square

3.4. Algorithm. The algorithm for choosing the exponential approximation space and the tension parameter is described as follows. Without great loss, we suppose that $H^{(n)}(x_{j+1/2})$ does not vanish simultaneously for both $n = 4, 5$.

Algorithm for choosing the tension parameter.

Let \mathcal{S}_5 be the 5-point stencil around the given evaluation point $\bar{x} = x_{j+1/2}$. From the given cell-average values \bar{h}_n on \mathcal{S}_5 , construct $H(x_{n+1/2})$ on the cell boundaries and evaluate $H^{(\ell)}(\bar{x})$ for $\ell = 4, 5, 6$ by using the ℓ th order divided difference around \bar{x} , denoted by $[H^{(\ell)}(\bar{x})]$.

0. If $[H^{(6)}(\bar{x})] = 0$, we use the classical method based on algebraic polynomials, i.e.,

$$\mathbb{B}_5 = \{x^n : n = 0, \dots, 4\}.$$

1. If $[H^{(4)}(\bar{x})] \neq 0$, we choose the set of exponential polynomials as $\mathbb{B}_5 = \{1, x, x^2, \sinh \lambda x, \cosh \lambda x\}$ with

$$\lambda^2 = [H^{(6)}(\bar{x})]/[H^{(4)}(\bar{x})].$$

3. If $[H^{(4)}(\bar{x})] = 0$ and $|[H^{(5)}(\bar{x})]| > 0$, we modify \mathbb{B}_5 as $\mathbb{B}_5 = \{1, x, x^2, \sinh \lambda x, \cosh \lambda x + \lambda^6 x^5/5!\}$ with

$$\lambda^2 = [H^{(6)}(\bar{x})]/[H^{(5)}(\bar{x})].$$

In practice, $H^{(4)}(\bar{x}) \neq 0$ almost everywhere, as long as the flux f is not constant or linear (more generally, polynomially changing) around \bar{x} . Hence, we suggest to implement the proposed algorithm mainly based on ‘Step 1’.

4. A WENO SCHEME IMPROVING FIFTH-ORDER ACCURACY

Let $x_{j+1/2}$ be a given cell-boundary point. The five-point stencil $\mathcal{S}_5 = \{x_{j-2}, \dots, x_{j+2}\}$ around $x_{j+1/2}$ is divided into three candidate substencils \mathcal{S}_k with $k = 0, 1, 2$ consisting of three points. A local numerical flux $\hat{f}^k(x)$ is computed in each substencil \mathcal{S}_k and these solutions are combined into a weighted average to define a final WENO approximation to the value $h_{j+1/2}$:

$$(39) \quad \hat{f}_{j+1/2} = \sum_{k=0}^2 \omega_k \hat{f}_{j+1/2}^k.$$

In WENO reconstruction, the nonlinear weights are required to be close to the optimal weights for each local solution in smooth areas to attain a maximal accuracy, while removing the contribution of stencils that contain a singular point. From this view point, we first introduce new optimal weights based on the space T_5 of exponential polynomials.

4.1. An optimal weights based exponential polynomials. For the given cell-average values on the stencil \mathcal{S}_5 , the (global) numerical flux $\hat{f}_{j+1/2}$ approximating $h_{j+1/2}$ can be expressed as

$$(40) \quad \hat{f}_{j+1/2} = \sum_{\ell=0}^4 C_\ell \bar{h}_{j-2+\ell}, \quad \text{with} \quad C_\ell := \Delta x \sum_{n=\ell}^4 L'_n(x_{j+1/2}).$$

The local solution $\hat{f}_{j+1/2}^k$ is also computed at each substencil \mathcal{S}_k with $k = 0, \dots, 3$ and it is of the form

$$(41) \quad \hat{f}_{j+1/2}^k = \sum_{\ell=0}^2 C_\ell^k \bar{h}_{j-2+k+\ell} \quad \text{with} \quad C_\ell^k = \Delta x \sum_{n=\ell}^2 u'_n(x_{j+1/2}).$$

It is necessary to remark that the local numerical flux is the same as the case of the classical fifth-order WENO scheme. Then the numerical flux $\hat{f}_{j+1/2}$ can be expressed as a convex combination of the local fluxes:

$$\hat{f}_{j+1/2} = d_0 \hat{f}_{j+1/2}^0 + d_1 \hat{f}_{j+1/2}^1 + d_2 \hat{f}_{j+1/2}^2$$

where $\{d_k\}$ are the so-called optimal (ideal) weights such that $d_0 + d_1 + d_2 = 1$. The optimal weights d_k , $k = 0, 1, 2$, for the proposed WENO scheme can be obtained as

$$(42) \quad d_0 = C_0/C_0^0, \quad d_1 = (C_1 - d_0 C_1^0)/C_0^1, \quad d_2 = 1 - d_0 - d_1.$$

Unlike the case of the classical WENO scheme, the optimal weights $\{d_k\}$ of the proposed WENO method may vary depending on the choice of the parameter λ but tends to the original ideal weights as $\Delta x \rightarrow 0$.

4.2. A New Nonlinear Weight. The smoothness indicator is one of the most important ingredient in WENO reconstruction because the nonlinear weights are determined by measuring the smoothness of the local solution on each substencil \mathcal{S}_k . In this section, we introduce a new set of nonlinear weights which improves the known fifth-order WENO schemes. We follow the methodology of the WENO-Z scheme but provide fundamental modifications. A new global smoothness indicator is incorporated into the local smoothness indicator which measures the approximate magnitude of the derivatives of the local solution on each substencil based on L^1 -norm [12]. Specifically, let $\mathbb{D}_{n,k}$ be the operators defined by

$$(43) \quad \begin{aligned} \mathbb{D}_{1,k} f &:= (1-k)f_{j-2+k} + (2k-3)f_{j-1+k} + (2-k)f_{j+k}, \\ \mathbb{D}_{2,k} f &:= f_{j-2+k} - 2f_{j-1+k} + f_{j+k}. \end{aligned}$$

Here, the operator $\mathbb{D}_{1,k} f$ is a generalized undivided difference of f which approximates $\Delta x f'$ at $x_{j+1/2}$ with higher convergence rate [12]:

$$(44) \quad \mathbb{D}_{1,k} f = f'(x_{j+1/2})\Delta x + \mathcal{O}(\Delta x^3).$$

Then the smoothness indicators β_k are defined as follows:

$$(45) \quad \beta_k := \theta |\mathbb{D}_{1,k} f| + |\mathbb{D}_{2,k} f|, \quad \xi \in (0, 1],$$

where the value θ is a balanced trade off between $\mathbb{D}_{1,k} f$ and $\mathbb{D}_{2,k} f$. Having performed numerical experiments with several alternatives, we take $\theta = 0.25$ for all test problems except the case of 1-D linear advection equation in which $\theta = 0.1$. A novel idea of the proposed nonlinear weights is to measure the higher order information of the numerical flux on the large stencil \mathcal{S}_5 by using the fourth-order undivided difference

$$\tau_5 := \mathbb{D}_4 f_j = f_{j-2} - 4f_{j-1} + 6f_j - 4f_{j+1} + f_{j+2}.$$

With these (local and global) smoothness indicators at hand, the (unnormalized) nonlinear weight α_k , $k = 0, 1, 2$, are computed as

$$(46) \quad \alpha_k = d_k \left(1 + \frac{\tau_5^2}{\beta_k^2 + \epsilon} \right), \quad \epsilon := \epsilon(\Delta x).$$

Here, $\epsilon > 0$ is usually employed to prevent the denominator from a division by zero but it in fact affects the order of accuracy of the WENO method especially at the critical points. The specific choice of ϵ will be discussed in Proposition 4.1. Then, the final weights ω_k are defined via the normalization process, i.e.,

$$(47) \quad \omega_k = \frac{\alpha_k}{\sum_{\ell=0}^2 \alpha_\ell}, \quad k = 0, 1, 2.$$

4.3. Convergence Order of WENO-H. It is basic to require that the numerical solution $\hat{f}_{j\pm 1/2}$ approximates the flux h in (3) with a suitable convergence order on smooth regions. For this, the nonlinear weights ω_k should converge to the optimal weights d_k as $\Delta x \rightarrow 0$. To attain the sixth-order accuracy of the numerical flux $\hat{f}_{j+1/2}$, the nonlinear weights need to satisfy the following sufficient condition (e.g., see [12])

$$(48) \quad \omega_k^\pm - d_k = O(\Delta x^4),$$

where superscript ‘ \pm ’ on the weight ω_k corresponds to their use in the substencils of the local solution $f_{j\pm 1/2}^k$ respectively. In what follows, we show that the new nonlinear weights ω_k fulfill the condition in (48). For this purpose, it is helpful to introduce the general form of β_k which can be obtained by using the Taylor expansion argument:

$$(49) \quad \begin{aligned} \beta_0 &= \theta \left| f'_{j+1/2} \Delta x - \frac{23}{24} f'''_{j+1/2} \Delta x^3 \right| + \left| f''_{j+1/2} \Delta x^2 - \frac{3}{2} f'''_{j+1/2} \Delta x^3 \right| + \mathcal{O}(\Delta x^4), \\ \beta_1 &= \theta \left| f'_{j+1/2} \Delta x + \frac{1}{24} f'''_{j+1/2} \Delta x^3 \right| + \left| f''_{j+1/2} \Delta x^2 - \frac{1}{2} f'''_{j+1/2} \Delta x^3 \right| + \mathcal{O}(\Delta x^4), \\ \beta_2 &= \theta \left| f'_{j+1/2} \Delta x + \frac{1}{24} f'''_{j+1/2} \Delta x^3 \right| + \left| f''_{j+1/2} \Delta x^2 + \frac{1}{2} f'''_{j+1/2} \Delta x^3 \right| + \mathcal{O}(\Delta x^4). \end{aligned}$$

Proposition 4.1. *Let d_k , $k = 0, 1, 2$, be the optimal weights in (42). Assume that $\epsilon = \epsilon(\Delta x)$ in the definition of α_k (46) is chosen as $\epsilon = \Delta x^\gamma$ with $0 < \gamma \leq 4$. If f is smooth around the global stencil \mathcal{S}_5 , then the weights ω_k in (47) satisfy the following condition*

$$|\omega_k - d_k| = \mathcal{O}(\Delta x^4)$$

even near the critical points.

Proof. Taking the Taylor expansion of f around $x_{j+1/2}$, we can find that there exists a positive integer $r \in \mathbb{N}$ such that each β_k in (49) can be expressed as

$$(50) \quad \beta_k = c |f_{j+1/2}^{(r)} \Delta x^r| + \mathcal{O}(\Delta x^{r+1})$$

with a constant $c > 0$ independent of f and Δx . Certainly, if $x_{j+1/2}$ is not a critical point of f , then $r = 1$. Moreover, the truncation of the global smoothness indicator τ_5 is of the form

$$(51) \quad \tau_5 = |f_{j+1/2}^{(4)} \Delta x^4| + \mathcal{O}(\Delta x^5).$$

Then, we first consider the case $2r \leq \gamma$. Substituting $\epsilon = \Delta x^\gamma$ in (46) and by using (50) and (51), it is straightforward that

$$(52) \quad \frac{\tau_5^2}{\beta_k^2 + \epsilon} = \frac{\tau_5^2}{\beta_k^2 + \Delta x^\gamma} = c_f \Delta x^{8-2r} \frac{1 + \mathcal{O}(\Delta x)}{1 + \mathcal{O}(\Delta x^{\gamma-2r})}$$

for some constant $c_f > 0$. By hypothesis, $0 < \gamma \leq 4$ and $2r \leq \gamma$ so that it yields the relation

$$(53) \quad \alpha_k = d_k \left(1 + \frac{\tau_5^2}{\beta_k^2 + \epsilon} \right) = d_k + \mathcal{O}(\Delta x^4).$$

Further, since $d_1 + d_2 + d_3 = 1$, putting (53) into (47) clearly verifies that $|d_k - \omega_k| = \mathcal{O}(\Delta x^4)$, regardless of the issue of the critical points. Also, in the case $2r > \gamma$, it can be proved similarly. Therefore, the proof is completed. \square

TABLE 1. L^1 and L^∞ approximation errors and orders of accuracy for the one-dimensional Euler equation (54) at $t = 4$.

	WENO-JS	WENO-M	WENO-Z	WENO-H
N	L^1 approximation error (order)			
50	3.98E-02 (—)	9.70E-03 (—)	9.62E-03 (—)	7.26E-03 (—)
100	1.86E-03 (4.42)	2.69E-04 (5.17)	2.75E-04 (5.13)	2.81E-05 (8.01)
200	5.85E-05 (4.99)	8.35E-06 (5.01)	8.36E-06 (5.04)	4.49E-07 (5.97)
400	1.83E-06 (5.00)	2.61E-07 (5.00)	2.61E-07 (5.00)	7.04E-09 (6.00)
800	5.71E-08 (5.00)	8.16E-09 (5.00)	8.16E-09 (5.00)	9.53E-11 (6.21)
N	L^∞ approximation error (order)			
50	6.03E-02 (—)	1.49E-02 (—)	1.49E-02 (—)	1.11E-02 (—)
100	2.71E-03 (4.47)	4.18E-04 (5.16)	4.49E-04 (5.05)	4.81E-05 (7.85)
200	9.81E-05 (4.79)	1.31E-05 (5.00)	1.34E-05 (5.07)	7.08E-07 (6.08)
400	3.28E-06 (4.90)	4.10E-07 (5.00)	4.12E-07 (5.02)	1.11E-08 (6.00)
800	1.03E-07 (5.00)	1.28E-08 (5.00)	1.28E-08 (5.00)	1.50E-10 (6.20)

TABLE 2. L^1 and L^∞ approximation errors and orders of accuracy for the two-dimensional Euler equation (54) at $t = 4$

	WENO-JS	WENO-M	WENO-Z	WENO-H
$N \times N$	L^1 approximation error (order)			
25×25	3.06E-01 (—)	2.70E-01 (—)	2.26E-01 (—)	2.03E-01 (—)
50×50	5.57E-02 (2.46)	1.40E-02 (4.27)	1.40E-02 (4.01)	1.06E-02 (4.26)
100×100	2.71E-03 (4.36)	4.01E-04 (5.13)	4.12E-04 (5.09)	1.43E-05 (9.54)
200×200	8.77E-05 (4.95)	1.25E-05 (5.00)	1.25E-05 (5.04)	2.28E-07 (5.97)
400×400	2.74E-06 (5.00)	3.91E-07 (5.00)	3.91E-07 (5.00)	3.54E-09 (6.01)
$N \times N$	L^∞ approximation error (order)			
25×25	4.81E-01 (—)	4.25E-01 (—)	3.54E-01 (—)	3.22E-01 (—)
50×50	8.20E-02 (2.55)	2.17E-02 (4.29)	2.17E-02 (4.03)	1.63E-02 (4.3)
100×100	3.75E-03 (4.45)	6.26E-04 (5.11)	6.67E-04 (5.02)	2.78E-05 (9.1)
200×200	1.42E-04 (4.72)	1.96E-05 (5.00)	2.00E-05 (5.06)	3.63E-07 (6.2)
400×400	4.75E-06 (4.90)	6.15E-07 (5.00)	6.18E-07 (5.02)	5.59E-09 (6.0)

4.4. **Accuracy test for smooth periodic Euler equations.** The goal of this subsection is to demonstrate the convergence rate of accuracy of the proposed WENO-H scheme. We especially show that the carefully chosen exponential approximation space can improve the accuracy of the WENO reconstruction. The desired order of accuracy of WENO-H is tested by solving the following Euler equation for one and two-dimensional cases:

$$(54) \quad U_t + F(U)_x + G(U)_y = 0,$$

with

$$U = \begin{bmatrix} \rho \\ \rho u \\ \rho v \\ E \end{bmatrix}, \quad F(U) = \begin{bmatrix} \rho u \\ p + \rho u^2 \\ \rho uv \\ u(p + E) \end{bmatrix} \quad \text{and} \quad G(U) = \begin{bmatrix} \rho v \\ \rho v u \\ p + \rho v^2 \\ v(p + E) \end{bmatrix}.$$

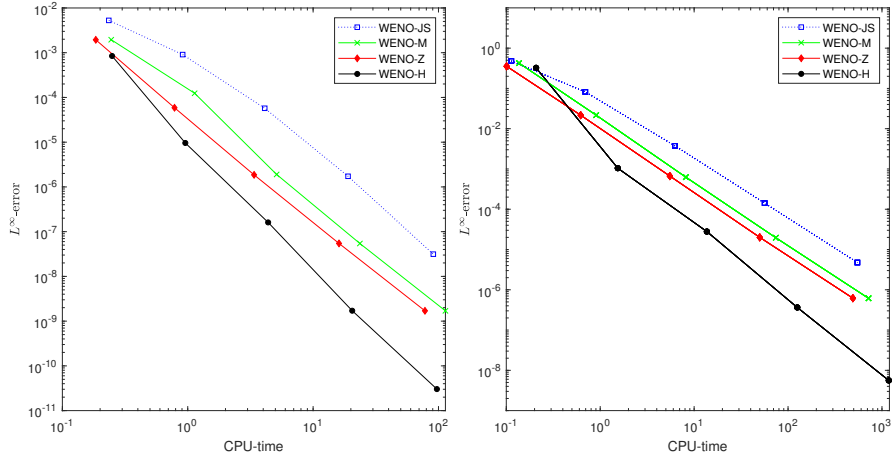


FIGURE 1. Numerical Efficiency (CPU time versus errors) for the one (left) and two-dimensional (right) Euler equations (54).

Here, ρ, u, v , and E indicate the density, particle velocities (along the x and y -directions), and total energy, respectively. The pressure p has a relation with the total energy, that is, ideal gas equation state:

$$E = \frac{p}{\gamma - 1} + \frac{\rho(u^2 + v^2)}{2}$$

with γ the ratio of specific heats. Here, we set $\gamma = 1.4$. The initial data is

$$\rho(x, y, t) = 1 + 0.5 \sin(4\pi(x + y))$$

with $u = 1$, $v = -1/2$, and $p = 1$. The exact solution on the unit square is

$$\rho(x, y, t) = 1 + 0.5 \sin(4\pi(x + y - t(u + v))),$$

and the periodic boundary conditions are employed. We perform the numerical simulation until the final time $t = 4$. For the time evolutions, we use non-TVD RK4 [37] with $\Delta t = \Delta x^{6/4}$. The numerical results of WENO-H and other well-known fifth-order WENO schemes are presented in Table 1 and Table 2 for one and two-dimensional problems respectively. The L^1 - and L^∞ -errors and convergence orders of density ρ are reported. In addition, we also compare the effectiveness of these WENO schemes by computing the CPU time versus L^∞ -error using various grids. In the comparison, the L^∞ -errors against CPU time are presented in Fig. 1 for one and two-dimensional problems. Each marker indicates ‘CPU time-errors’ at 50×2^k and $(25 \cdot 2^k) \times (25 \cdot 2^k)$ grid points for one and two-dimensional cases with $k = 0, 1, 2, 3, 4$. The WENO-H scheme shows better efficiency compared to other WENO schemes.

5. NUMERICAL RESULTS

In this section, we provide some experimental results to illustrate the performance of the WENO-H scheme. The experimental results of the WENO-H scheme are compared with those of other well-known fifth-order WENO schemes: WENO-JS, WENO-M and WENO-Z. For the evaluation of the shock capturing abilities of the proposed algorithm, the simulations are performed for several benchmarks of one and two-dimensional scalar and system of conservation laws. For all the numerical experiments in this section, we employ the third-order TVD Runge-Kutta-type discretization for time evolution.

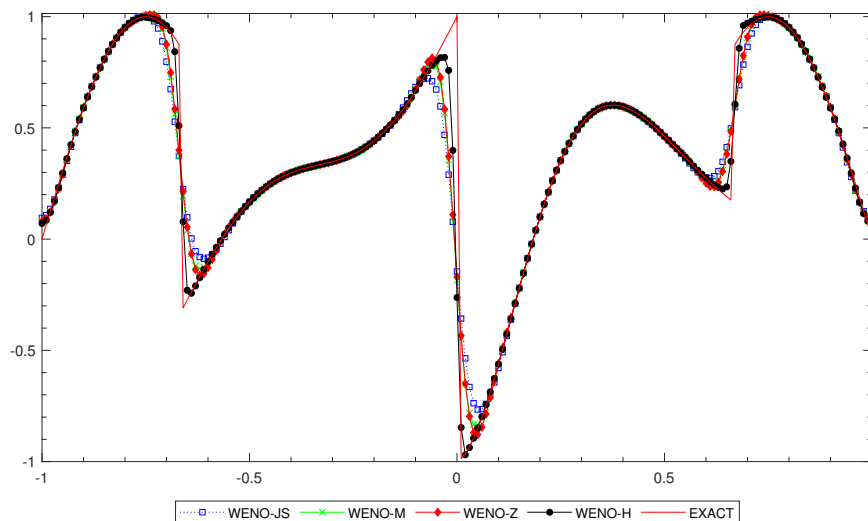


FIGURE 2. Comparison of the analytic solution with the numerical results of the advection equation with initial conditions (56) with WENO-JS, WENO-M, WENO-Z, and WENO-H at $t = 11$ with 200 grid points.

5.1. Scalar Test Problems. We investigate the behavior of the WENO-H method for the one-dimensional advection equation with an initial data including unusual edges and contact discontinuities.

Example 5.1. (Linear equation) Let us solve the advection equation:

$$(55) \quad q_t + q_x = 0, \quad t \in \mathbb{R}^+$$

with the initial condition specified as

$$(56) \quad q(x, 0) = q_0(x) = \begin{cases} -x \sin(\frac{3\pi}{2}x^2) & \text{for } x \in [-1, -\frac{1}{3}], \\ |\sin(2\pi x)| & \text{for } x \in (-\frac{1}{3}, \frac{1}{3}), \\ 2x - 1 - \frac{1}{6} \sin(3\pi x) & \text{for } x \in (\frac{1}{3}, 1]. \end{cases}$$

We set the periodic boundary conditions and carry out the computation until the final time $t = 11$ with $\Delta x = 0.01$. The CFL condition number is 0.4. The numerical results of this advection equation with initial condition (56) are shown in Fig. 2. We observe that the WENO-H method has smaller errors than other WENO fifth-order schemes near the singular points.

5.2. One-dimensional Euler Systems. Let us consider the one-dimensional Euler gas dynamics for ideal gases. The characteristic decomposition is performed to generalize the WENO methods [38].

Example 5.2. We apply the WENO-H scheme to the shock-density wave interaction test problem that describes shock interacting with entropy waves. This model problem was introduced by Shu and Osher [37] to test the capability of a high-order WENO scheme to capture the high frequency waves. The solution of this example includes large scale waves, small shocks and fine scale structures. We solve this problem on the interval $[-5, 5]$ with the specified initial condition:

$$(\rho, u, p) = \begin{cases} (3.857143, 2.629369, 10.33333) & \text{for } x \in [-5, -4), \\ (1 + \varepsilon \sin(kx), 0, 1) & \text{for } x \in [-4, 5] \end{cases}$$

where $\varepsilon = 0.2$ is the amplitude of the entropy wave and k is wave number of the entropy wave. A shock wave flowing to the right (with speed ‘Mach 3’) interacts sine wave in a perturbed density disturbance such that it yields a flow field with discontinuities as well as smooth structures. We simulate this problem for

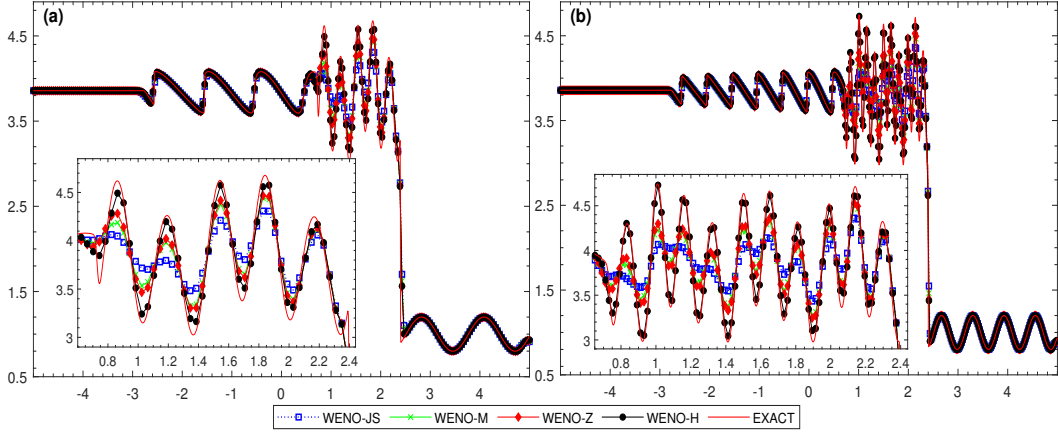


FIGURE 3. Density profiles of the shock-entropy interacting of Shu-Osher [37] by WENO-JS, WENO-M, WENO-Z, and WENO-H. (a) $t = 1.8$ with 250 grid points for $k = 5$, (b) $t = 1.8$ with 500 grid points for $k = 10$.

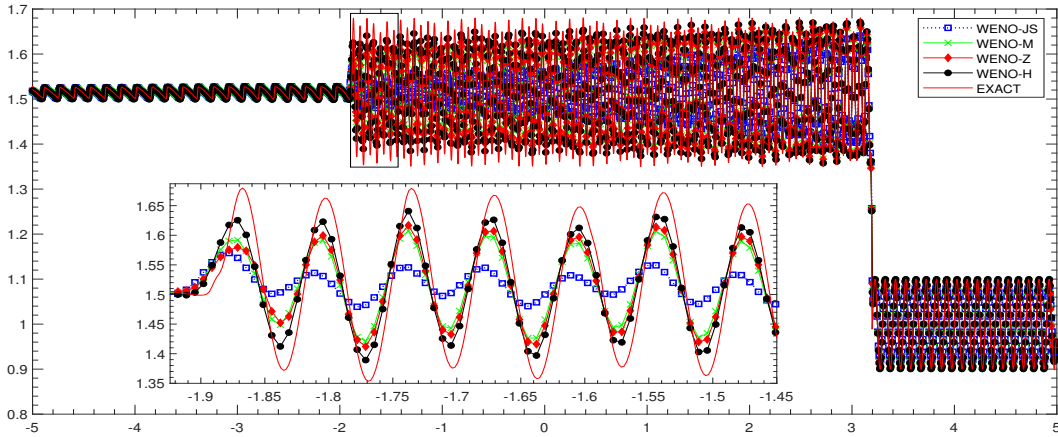


FIGURE 4. Numerical results with WENO-JS, WENO-M, WENO-Z, and WENO-H at $t = 5$ with 1500 grid points.

$k = 5, 10$ until the output time $t = 1.8$ using the CFL number 0.5. The exact solution of this model problem is unknown. So, the reference solution is computed by the classical fifth-order WENO-JS scheme with 3200 points. Fig. 3 plots a comparison of the densities ρ for all schemes at time $t = 1.8$. Notice that WENO-H resolves most of the waves with a good accuracy (to their amplitudes) over other tested methods.

In addition, as a variation of the Shu-Osher problem, let us solve Titarev-Toro problem with the initial condition given as follows [42]:

$$(\rho, u, p) = \begin{cases} (1.515695, 0.523346, 1.80500) & \text{for } x \in [-5, -4), \\ (1 + 0.1 \sin(20\pi x), 0, 1) & \text{for } x \in [-4, 5]. \end{cases}$$

The simulation is performed up to time $t = 5$ with $\Delta x = 1/150$. Fig. 4 shows the numerical solutions on a grid with 1500 grid points (i.e., $\Delta x = 1/150$) for all the computed WENO schemes. We observe that the oscillatory wave pattern behind shock entropy wave interactions is well captured by WENO-H better than other WENO methods.

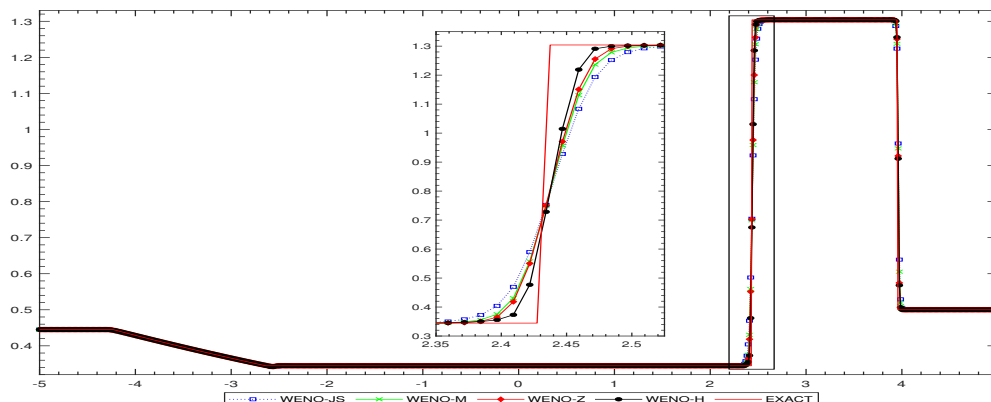


FIGURE 5. Numerical results of Lax problem [26] with WENO-JS, WENO-M, WENO-Z, and WENO-H at $t = 1.6$ with 200 grid points.

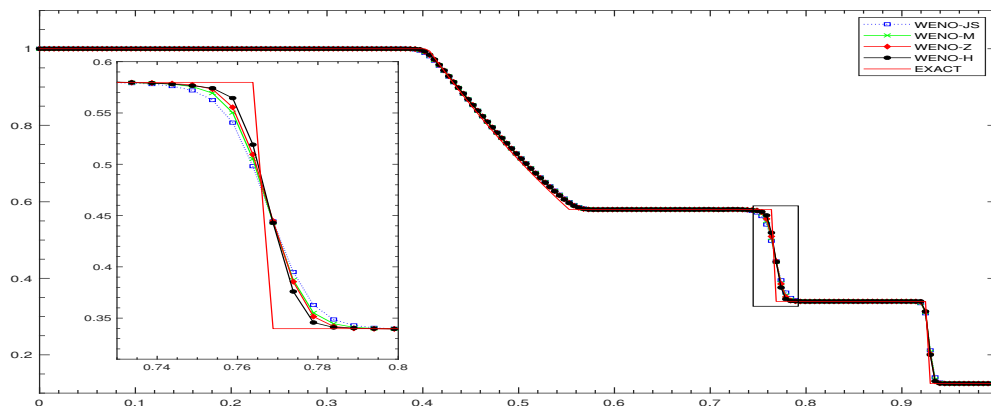


FIGURE 6. Numerical results of Sod problem [40] with WENO-JS, WENO-M, WENO-Z, and WENO-H at $t = 0.2$ with 200 grid points.

Example 5.3. We test one-dimensional Euler equation for the Lax problem [26]. The initial condition is specified by

$$(\rho, u, p) = \begin{cases} (.445, .698, 3.528) & \text{for } x \in [-5, 0), \\ (.5, 0, .571) & \text{for } x \in [0, 5] \end{cases}$$

with $\gamma = 1.4$. The computation is performed up to time $t = 0.16$ with 200 grid points (i.e., $\Delta x = 1/20$). Fig. 5 presents the exact solution (reported in Toro [41]) and the density ρ profiles obtained by several WENO schemes. The result of WENO-H is closer to the exact solution and captures the shock and contact transitions nearby discontinuities better than other WENO schemes.

Example 5.4. In this example, we solve the one-dimensional Euler equation for the Sod problem [40] with the Riemann initial condition given by

$$(\rho, u, p) = \begin{cases} (1, 0.75, 1) & \text{for } x \in [0, 0.5), \\ (0.125, 0, 0.1) & \text{for } x \in [0.5, 1] \end{cases}$$

with $\gamma = 1.4$. The computation has been performed up to time $t = 0.2$. The computed density distributions and exact solution are shown in Fig. 6 with 200 grid points (i.e. $\Delta x = 1/200$). The exact solution is

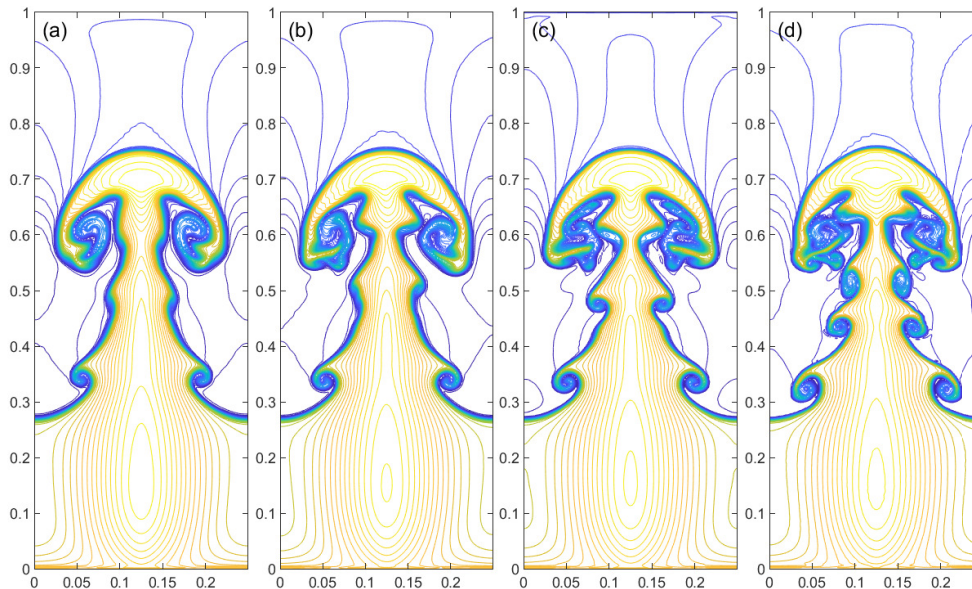


FIGURE 7. Two-dimensional Rayleigh-Taylor instability [34, 44]: (a) WENO-JS, (b) WENO-M, (c) WENO-Z, and (d) WENO-H at $t = 1.95$ with 120×480 grid points.

obtained by using the exact Riemann solver [41]. One can see that the solution of WENO-H well captures the shock and contact discontinuity without redundant oscillations better than WENO-JS, WENO-M and WENO-Z do.

5.3. Two-dimensional Euler Systems. The numerical results of two-dimensional compressible Euler equations are provided in this section. We specify an initial condition for each test problem and set $\gamma = 1.4$ except the two-dimensional Rayleigh-Taylor instability problem.

Example 5.5. (Two-dimensional Rayleigh-Taylor instability) This model problem describes the interface instability between fluids with different densities, where the heavy fluid moves down to the light fluid. This problem has been computed to check the numerical dissipation (e.g., [34, 44]). In this example, the simulation is performed on the domain $[0, 0.25] \times [0, 1]$ with the initial condition specified by

$$(\rho, u, v, p) = \begin{cases} (2, 0, -0.025\sqrt{\frac{5p}{3\rho}} \cos(8\pi x), 2y + 1) & \text{for } y \in [0, 0.5), \\ (1, 0, -0.025\sqrt{\frac{5p}{3\rho}} \cos(8\pi x), 2y + 1.5) & \text{for } y \in [0.5, 1]. \end{cases}$$

The gravitational effect can be obtained by adding ρ and ρv to the right of y -momentum and the energy equation respectively. We set the ratio of specific heats as $\gamma = 5/3$. The right and left-hand boundaries are taken by the reflective boundary conditions. The velocity is 0, and we set $(\rho, p) = (1, 2.5)$ for the top boundary condition and $(\rho, p) = (2, 1)$ for the bottom boundary condition. The results are simulated up to time $t = 1.95$. Fig. 7 depicts the density contour lines of the solutions computed by the WENO-H and other fifth-order WENO schemes with 120×480 grid points. The appearance of the small structure in the flow is a measure of the small magnitude of the intrinsic numerical viscosity of the numerical schemes. We can observe that the WENO-H scheme is able to capture complex structures better than other schemes and improves significantly the contact discontinuity resolution.

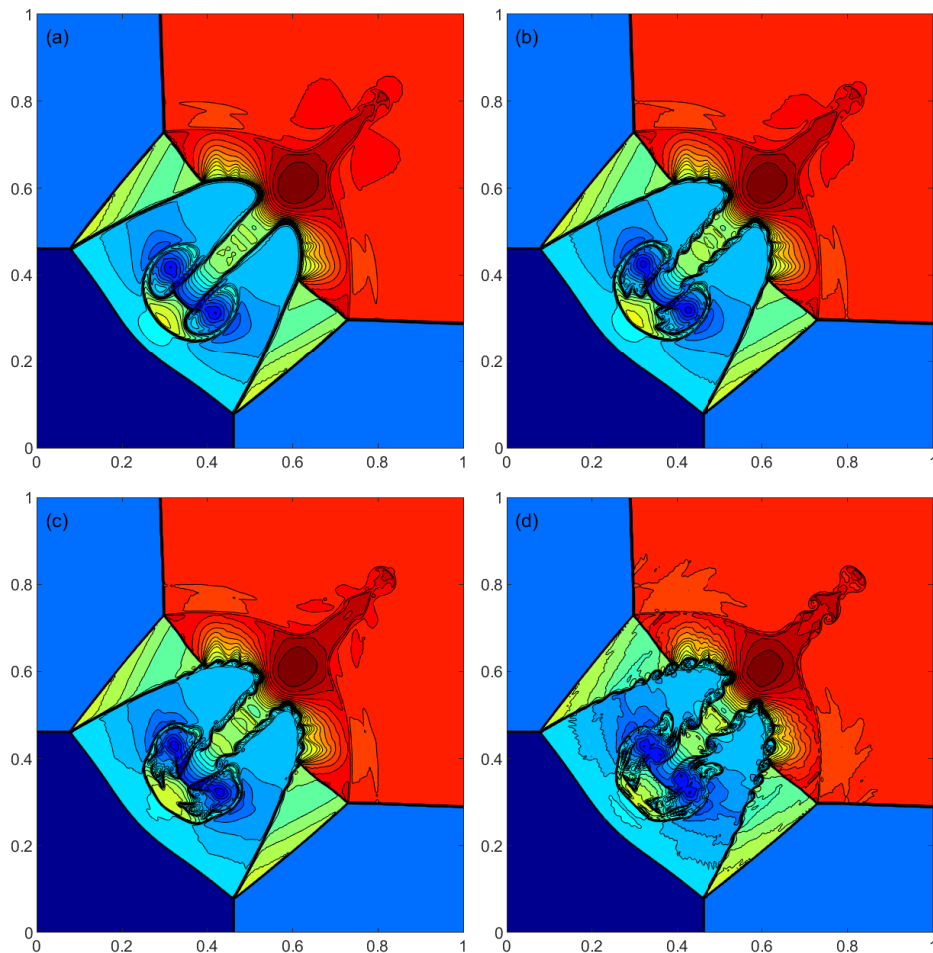


FIGURE 8. Density profiles of two-dimensional problem [33]: (a) WENO-JS, (b) WENO-M, (c) WENO-Z, (d) WENO-H at $t = 0.8$ with 500×500 grid points.

Example 5.6. (Two-Dimensional Riemann Problem for Gas Dynamics) We consider the third configuration of the two-dimensional Riemann problems for gas dynamics [33]. The computational domain is $[0, 1] \times [0, 1]$ which is divided into 4 quadrants by lines $x = 0.8$ and $y = 0.8$. In each quadrant, the initial data is set as constant:

$$(\rho, u, v, p) = \begin{cases} (1.5, 0, 0, 1.5) & \text{for } (x, y) \in [0.8, 1] \times [0.8, 1], \\ (0.5323, 1.206, 0, 0.3) & \text{for } (x, y) \in [0, 0.8] \times [0.8, 1], \\ (0.138, 1.206, 1.206, 0.029) & \text{for } (x, y) \in [0, 0.8] \times [0, 0.8], \\ (0.5323, 0, 1.206, 0.3) & \text{for } (x, y) \in [0.8, 1] \times [0, 0.8] \end{cases}$$

with outflow boundary conditions. The computation is carried out until time $t = 0.8$ with 500×500 grid points. The performance of WENO-H is compared with those of other WENO schemes in Figs. 8.

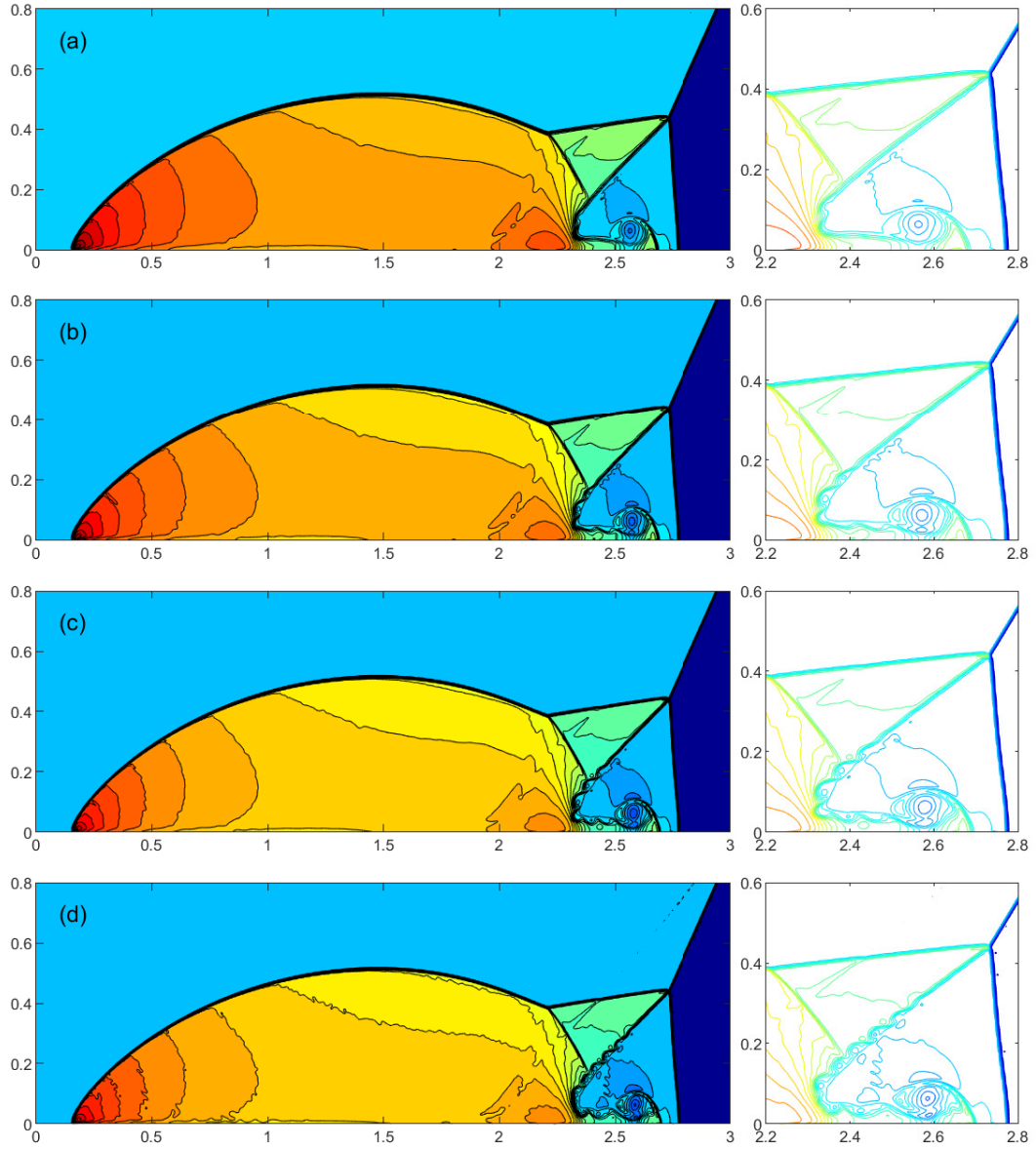


FIGURE 9. Double Mach reflection of a strong shock [43]: (a) WENO-JS, (b) WENO-M, (c) WENO-Z, (d) WENO-H at $t = 0.2$ with 960×240 .

Example 5.7. (Double Mach reflection of a strong shock) This model problem was introduced by Woodward and Colella [43]. Since then, it has been used to test the capability of a high accurate scheme to capture small-scale structures and shocks. We test this problem on the domain $[0, 4] \times [0, 1]$. This example is initialized with a right-moving Mach 10 oblique shock oriented at an angle of 60° to the horizontal axis

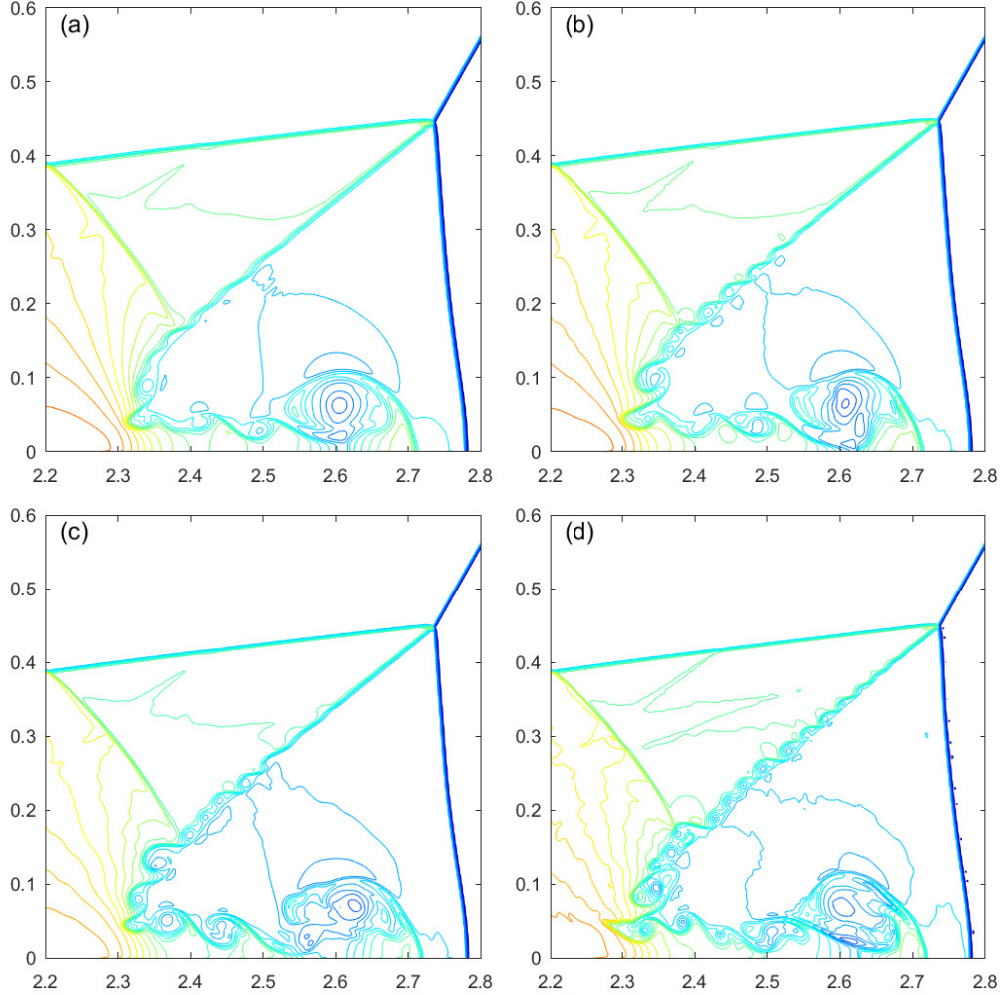


FIGURE 10. Double Mach reflection of a strong shock [43]: (a) WENO-JS, (b) WENO-M, (c) WENO-Z, and (d) WENO-H at $t = 0.2$ with 1920×480 grid points.

passing through the point $(x, y) = (\frac{1}{6}, 0)$. Exact post-shock condition is used for the boundary conditions on $x \in [0, \frac{1}{6}]$ and the rest part of the bottom is used as a reflective boundary condition. Left and right boundaries use inflow and outflow boundary conditions. Exact motions of the Mach 10 shock are used to the boundary of top parts. Density $\rho = 1.4$ and pressure $p = 1$ are set for the unshocked fluid. The problem was run till $t = 0.2$. Fig. 9 and 10 plot the density profiles computed with the WENO-H and WENO-JS, WENO-M and WENO-Z schemes with 960×240 and 1920×480 grid points respectively. We can see that the WENO-H scheme yields better resolutions than other WENO methods.

Example 5.8. (A Mach 3 Wind Tunnel with a Step) This problem describes a Mach 3 flow with a forward-facing step in a wind tunnel. It was first described by Emery [7] to compare several hydrodynamical methods. Later, Woodward and Colella [43] used it to compare several advanced numerical schemes. We compute

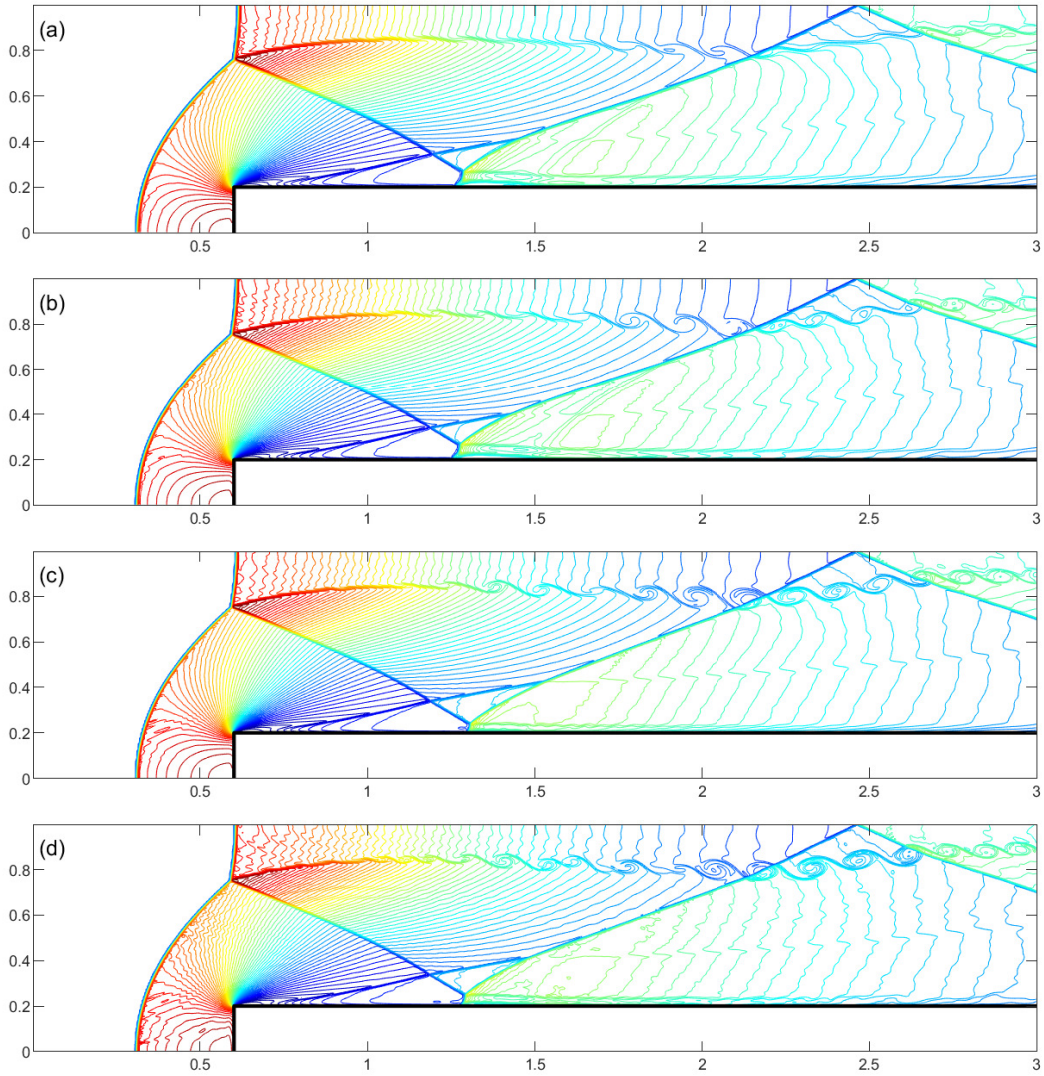


FIGURE 11. Density profiles of Mach 3 Wind tunnel with a step [43]: (a) WENO-JS, (b) WENO-M, (c) WENO-Z, and (d) WENO-H at $t = 4$ with 768×256 grid points.

this problem in a wind tunnel with one length unit width and three length units long. The step is 0.2 length units high and is located 0.6 length units from the left-hand end of the tunnel. The reflective boundary conditions is assumed along the walls of the tunnel. We also assume that the tunnel has an infinite width along the direction orthogonal to the calculation plane. A gas is continuously supplied at the left boundary with the pressure 1, density 1 and velocity 3 respectively. The corner of the step is the singularity of the flow, since it is the center point of the rarefaction fan. After the bow shock is reflected in the step, the shock gradually reaches the top reflective wall of the tunnel around $t = .65$. Due to the reflections and interactions of the shocks, a triple point is formed, from which the trail of vortices moves towards the right boundary. Fig. 11 plots the density profiles obtained by WENO-H with the other WENO schemes at the final time $t = 4$ with 768×256 mesh grids. We see that the roll-up of the vortex sheet is more clearly visible with WENO-H.

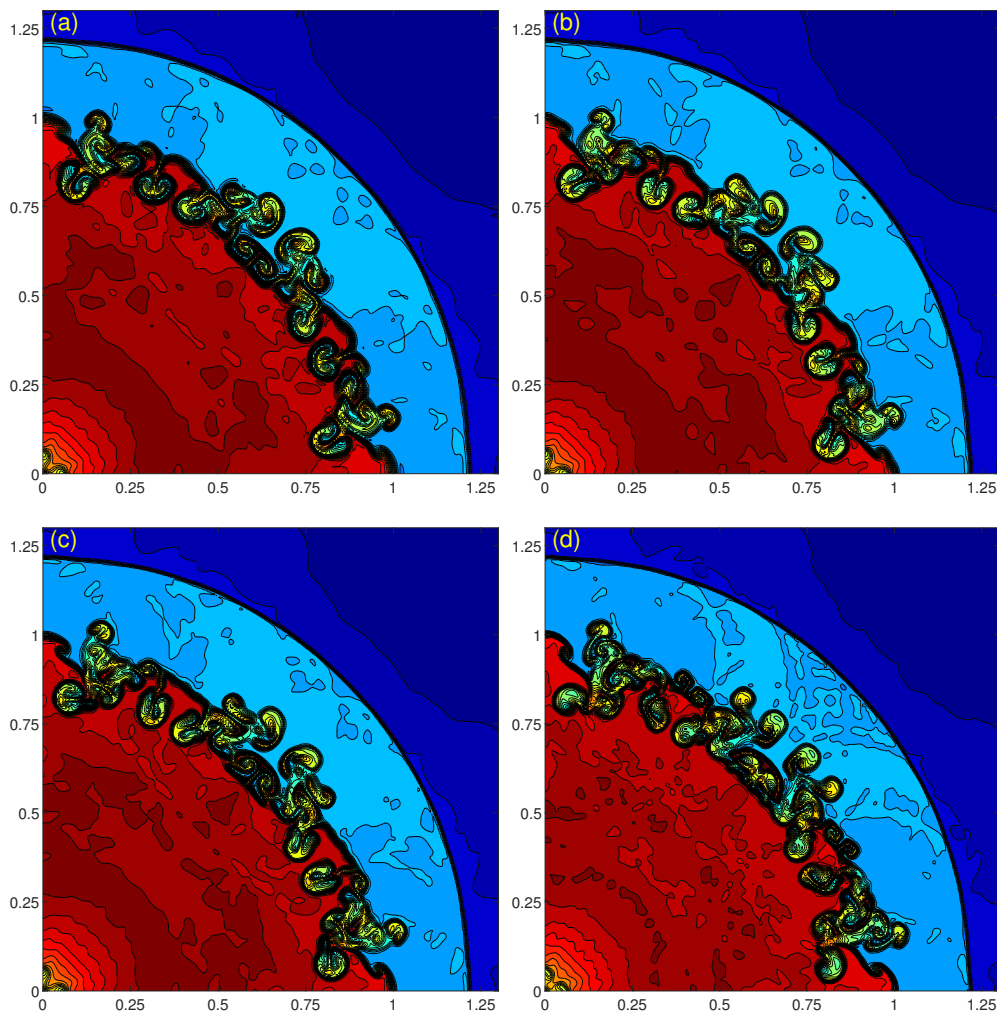


FIGURE 12. Density profiles of the first quadrant for Explosion [41], (a) WENO-JS, (b) WENO-M, (c) WENO-Z, and (d) WENO-H at $t = 3.2$.

Example 5.9. (Explosion) We compute the explosion problem proposed in [41] (see also [29]) which is a circularly symmetric two-dimensional problem with initial circular region of higher density and pressure. The circle is centered at the origin with radius 0.4. The computation is performed on the domain $[-1.5, 1.5] \times [-1.5, 1.5]$ with the initial condition given by

$$(\rho, u, v, p) = \begin{cases} (1.000, 0, 0, 1.0) & \text{if } x^2 + y^2 < 0.16, \\ (0.125, 0, 0, 0.1) & \text{otherwise} \end{cases}$$

with $\gamma = 1.4$. We compute the solution until time $t = 3.2$ with 600×600 mesh grids. Fig. 12 shows the density profiles obtained by the four tested WENO schemes. We can see that the numerical results by WENO-H are much ‘curlier’ at the contact surface than the results obtained by other tested methods. This explains that WENO-H has substantially smaller dissipation than other WENO schemes.

6. CONCLUSION

In this paper, we have proposed an improved WENO schemes (called WENO-H) for the numerical solution of the hyperbolic conservation laws. The interpolation method is based on the space of exponential polynomials with a tension parameter. We proposed a practical approach to determine the parameter of the exponential approximation space by taking into account the local data feature. As a result, the proposed WENO scheme attains an improved order of accuracy (that is, sixth-order) better than other fifth-order WENO methods without loss of accuracy at critical points. A detailed analysis is provided to verify the improved accuracy. Further, modified nonlinear weights based on L^1 -norm approach were proposed along with a new global smoothness indicator. The proposed WENO scheme resolve discontinuities sharply while reducing numerical dissipation significantly. Several experimental results of the WENO-H scheme for the advection equation and the system of the Euler equations are compared with those of the other fifth-order WENO scheme to confirm the reliability of the method. In the near future we generalized our approach to sixth or higher-order WENO schemes.

REFERENCES

- [1] F. Acker, R. B. de R. Borges and B. Costa, An improved WENO-Z scheme *J. Comput. Phys.* 313, 726-753 (2016).
- [2] D.S. Balsara, S. Garain, C.-W. Shu, An efficient class of WENO schemes with adaptive order, *J. Comput. Phys.* 326, 780804 (2016).
- [3] D.S. Balsara and C.W. Shu, Monotonicity preserving WENO schemes with increasingly high-order of accuracy, *J. Comput. Phys.* 160, 405–452 (2000).
- [4] R. Borges, M. Carmona, B. Costa, and W.S. Don, An improved WENO scheme for hyperbolic conservation laws, *J. Comput. Phys.* 227, 3191–3211 (2008).
- [5] I. Cravero, M. Semplice, On the accuracy of WENO and CWENO reconstructions of third order on nonuniform meshes, *J. Sci. Comput.* 67(3), 12191246 (2016).
- [6] L. L. Chen, C. Huang, An improved WLS-WENO method for solving hyperbolic conservation laws, *J. Comput. Phys.* 392, 96–114 (2019).
- [7] A. F. Emery, An Evaluation of several differencing methods for inviscid fluid flow problems, *J. Comput. Phys.* 2, 306–331 (1968).
- [8] G. H. GOLUB AND C. F. VAN LOAN, *Matrix Computations*, John Hopkins University Press. Baltimore, (1996).
- [9] S. Gottlieb, J. S. Mullen, and S.J. Ruuth, A Fifth Order Flux Implicit WENO Method, *J. Sci. Comput.* 27 (1-3), 271-287 (2006).
- [10] G.A. Gerolymos, D.Sénéchal, and I. Vallet, Very-high-order WENO schemes, *J. Comput. Phys.* 228, 8481–8524 (2009).
- [11] Y. Ha, Y.J. Lee and J. Yoon, Modified essentially non-oscillatory scheme based on exponential polynomial interpolation for hyperbolic conservation laws, *SIAM J. Numer. Anal.* 52 (2), 864-893 (2013).
- [12] Y. Ha, C. H. Kim, Y. J. Lee, and J. Yoon, An improved weighted essentially non-oscillatory scheme with a new smoothness indicator, *J. Comput. Phys.*, 232, 68–86(2013).
- [13] Y. Ha, C. H. Kim, Y. H. Yang, and J. Yoon, Sixth-order weighted essentially non-oscillatory schemes based on exponential polynomials, *SIAM J. Sci. Comput.*, Vol. 38, No 4, A1987–A2017(2016).
- [14] A. Harten, High resolution schemes for hyperbolic conservation laws, *J. Comput. Phys.*, 49, 357–393(1983).
- [15] A. Harten, On a Class of High Resolution Total-Variation-Stable Finite-Difference Schemes, *SIAM J. Numer. Anal.*, Vol. 21, no. 1, 1–23 (1984).
- [16] A. Harten, S. Osher, Uniformly High-order Accurate Non-oscillatory Schemes, *IMRC Technical Summary Rept. 2823*, Univ. of Wisconsin, Madison, WI, May 1985.
- [17] A. Harten and S. Osher, Uniformly High-Order accurate Non-Oscillatory schemes I. *SIAM J. Numer. Anal.* Vol. 24, No. 2, 279–309 (1987).
- [18] A. Harten, B. Engquist, S. Osher, and S. Chakravarthy, Uniformly High-Order accurate Non-Oscillatory schemes III. *J. Comput. Phys.* 131, 3–47(1997).
- [19] A.K. Henrick, T.D. Aslam, and J.M. Powers, Mapped weighted-essentially-non-oscillatory schemes : achieving optimal order near critical points, *J. Comput. Phys.* 207, 542–567 (2005).
- [20] X. Y. Hu Q. Wang, and N. A. Adams, An adaptive central-upwind weighted essentially non-oscillatory scheme, *J. Comput. Phys.*, 229, 8952–8965 (2010).
- [21] X. Y. Hu, and N. A. Adams, Scale separation for implicit large eddy simulation, *J. Comput. Phys.*, 230, 7240–7249 (2011).
- [22] G. Jiang and C.W. Shu, Efficient implementation of weighted ENO schemes, *J. Comput. Phys.* 126, 202–228 (1996).
- [23] S. Karlin and W.J. Studden, *Chebyshev Systems: With Applications in Analysis and Statistics*, Interscience Publishers, New York, 1966.

- [24] M. Käser, A. Iske, ADER schemes on adaptive triangular meshes for scalar conservation laws, *J. Comput. Phys.* 205, 486–508 (2005).
- [25] C. H. Kim, Y. Ha, and J. Yoon, Modified nonlinear weights for fifth-order weighted essentially non-oscillatory schemes, *J. Sci. Comput.*, 67, 299–323 (2016).
- [26] P.D. Lax, Weak solutions of Nonlinear Hyperbolic Equations and their Numerical Computation *Commun. Pure Appl. Math.* 7, 159–193 (1954).
- [27] D. Levy, G. Puppo, G. Russo, Central WENO schemes for hyperbolic systems of conservation laws, *M2AN. Math. Model. Numer. Anal.* 33, 547–571 (1999).
- [28] D. Levy, G. Puppo, G. Russo, Compact central WENO schemes for multidimensional conservation laws, *SIAM J. Sci. Comput.* 22, 656672 (2000).
- [29] R. Liska and B. Wendroff, Comparison of several difference schemes on 1D and 2D test problems for the Euler equations, *SIAM J. Sci. Comput.*, 25, 995–1017 (2004).
- [30] X.-D. Liu, S. Osher, and T. Chan, Weighted essentially non-oscillatory schemes, *J. Comput. Phys.* 115, 200–212 (1994).
- [31] H.X. Liu, X.M. Jiao, WLS-ENO: weighted-least-squares based essentially non-oscillatory schemes for finite volume methods on unstructured meshes, *J. Comput. Phys.* 314 749–773 (2016).
- [32] S. Pirozzoli, Conservative hybrid compact-WENO schemes for shock-turbulence interaction, *J. Comput. Phys.* 178, 81117 (2002).
- [33] C.W. Schulz-Rinne, J.P. Collins, and H.M. Glaz, Numerical Solution of the Riemann Problem for Two-Dimensional Gas Dynamics, *SIAM J. Sci. Comput.*, Vol. 14, No. 6, 1394–1414 (1993).
- [34] J. Shi, Y.T. Zhang, C.W. Shu, Resolution of high order WENO schemes for complicated flow structures *J. Comput. Phys.* 186, 690–696 (2003).
- [35] C.W. Shu, Essentially non-oscillatory and weighted essentially non-oscillatory schemes for hyperbolic conservation laws, in *Advanced Numerical Approximation of Nonlinear Hyperbolic Equations*, (Editor: A. Quarteroni), Lecture Notes in Mathematics, vol 1697, Springer-Verlag, Berlin/New York, 1998, 325–432.
- [36] C.W. Shu and S. Osher, Efficient implementation of essentially non-oscillatory shock capturing schemes, *J. Comput. Phys.* 77, 439–471 (1988).
- [37] C.W. Shu and S. Osher, Efficient implementation of essentially non-oscillatory shock capturing schemes II, *J. Comput. Phys.* 83, 32–78 (1989).
- [38] C.W. Shu, ENO and WENO schemes for hyperbolic conservation laws, in: B. Cockburn, C. Johnson, C.W. Shu, E. Tadmor (Eds.), *Advanced Numerical Approximation of Nonlinear Hyperbolic Equations*, Lecture Notes in Mathematics, vol. 1697, Springer, Berlin, 1998, pp. 325–432 (also NASA CR- 97-206253 and ICASE-97-65 Rep., NASA Langley Research Center, Hampton [VA, USA]).
- [39] Y. Q. Shen, G.W. Yang, Hybrid finite compact-WENO schemes for shock calculation, *Int. J. Numer. Methods Fluids* 53, 531560 (2007).
- [40] G. Sod, A Survey of Several Finite Difference Methods for Systems of Nonlinear Hyperbolic Conservation Laws, *J. Comput. Phys.* 27, 1–31 (1978).
- [41] E.F. Toro, *Riemann Solvers and Numerical Methods for Fluid Dynamics*, Springer-Verlag, New York, 1997.
- [42] V. A. Titarev and E. F. Toro, Finite volume WENO schemes for three-dimensional conservation laws, *J. Comput. Phys.* 201 (2014) 238–260.
- [43] P. Woodward and P. Colella, The Numerical Simulation of Two-Dimensional Fluid Flow with Strong Shocks, *J. Comput. Phys.* 54, 115–173 (1984).
- [44] Z.F. Xu, C.W. Shu, Anti-diffusive flux corrections for high order finite difference WENO schemes, *J. Comput. Phys.* 205, 458–485 (2005).
- [45] L. Yuan and C.W. Shu, Discontinuous Galerkin method based on non-polynomial approximation spaces, *J. Comput. Phys.* 218, 295–323 (2006).
- [46] R. Zhang, M. Zhang, C.-W. Shu, On the order of accuracy and numerical performance of two classes of finite volume WENO schemes, *Commun. Comput. Phys.* 5, 836848 (2009)
- [47] J. Zhu and J. Qiu, Trigonometric WENO schemes for hyperbolic conservation laws and highly oscillatory problems, *Commun. Comput. Phys.* 8, 1242–1263 (2010).
- [48] J. Zhu and J. Qiu, WENO schemes and their application as limiters for RKDG methods based on Trigonometric approximation spaces, *J. Sci. Comput.* 55, 606–644 (2013).
- [49] J. Zhu, J.X. Qiu, A new fifth order finite difference WENO scheme for solving hyperbolic conservation laws, *J. Comput. Phys.* 318, 110–121 (2016).
- [50] J. Zhu, J.X. Qiu, A new type of finite volume WENO schemes for hyperbolic conservation laws, *J. Sci. Comput.* 73, 1338–1359 (2017).